

Regularized 13-Moment Equations for Inverse Power Law Models

Zhenning Cai*, Yanli Wang†

December 9, 2019

Abstract

We propose a systematic methodology to derive the regularized thirteen-moment equations in the rarefied gas dynamics for a general class of linearized collision models. Detailed expressions of the moment equations are written down for all inverse power law models as well as the hard-sphere model. By linear analysis, we show that the equations are stable near the equilibrium. The models are tested for shock structure problems to show its capability to capture the correct flow structure in strong nonequilibrium.

Keywords: regularized 13-moment equations, inverse power law, shock structure

1 Introduction

Modeling of gas dynamics has been attracting people’s attention for centuries. Even for the simplest single-species, monatomic gas, while the classical continuum models such as Euler equations and Navier-Stokes-Fourier equations work well in most circumstances, people do find them inadequate when we care about some “extreme cases”, such as low-density regime and large velocity slip or temperature jump at a solid wall due to gas-surface interaction. In these cases, the interaction between gas molecules are either insufficient or severely ruined by gas-surface interactions, resulting in the failure of the continuum models. Although some microscopic models, such as Boltzmann equation, Enskog equation, or even molecular dynamics, have been validated to be accurate for most applications, they are usually too expensive to solve due to the high dimensionality. Despite the fast computers developed nowadays, a full three-dimensional simulation of the Boltzmann equation still requires a huge amount of computational resources [15], and therefore lower-dimensional models are preferable for slip or early-transitional flows. Since there is a large gap between the continuum models and the microscopic models, researchers have been trying to find models sitting in-between, which are cheaper to simulate than the kinetic models.

Since Euler equations and Navier-Stokes equations can be considered as zeroth-order and first-order approximations of the Boltzmann equation in the continuum limit [34], various attempts have been made to derive higher-order approximations. For example, by Chapman-Enskog expansion [17, 13], one obtains Burnett equations and super Burnett equations as third- and fourth-order approximations [7, 32, 33]; by Grad’s expansion, equations for stress tensor and heat fluxes can be derived to provide better closure than the Navier-Stokes and Fourier laws so that the models are suitable for a wider range of Knudsen numbers [18, 19]; by the assumption of maximum entropy, Euler equations can be extended to include 14 (or more) moments

*Department of Mathematics, National University of Singapore, Level 4, Block S17, 10 Lower Kent Ridge Road, Singapore 119076, email: matcz@nus.edu.sg.

†Beijing Computational Science Research Center, Beijing, China, 100193, email: wang-yanli@csrc.ac.cn.

[30, 16, 26]. However, these attempts show that going beyond Navier-Stokes is quite nontrivial: Burnett and super Burnett equations are linearly unstable [4]; Grad's method has the hyperbolicity problem and the convergence problem [8, 30]; equations by maximum entropy are still difficult to solve numerically due to an ill-posed optimization problem hidden in the equations [39]. These deficiencies have been severely restricting the applications of these models.

In spite of this, a number of new thoughts have been introduced for this classical modeling problem. In the current century, all these classical models are re-studied. Burnett equations have been fixed to regain linear stability [5, 6]; the hyperbolicity problem of Grad's equations is fixed in [9]; approximations of maximum-entropy equations have been proposed which have explicit analytical expressions [27]. At the same time, Grad's old idea hidden in his notes [19] has been picked up to build new models called regularized moment equations [36]. Although all these models are quite new, based on current studies, we find the regularized moment equations to be interesting due to its relatively complete theory (boundary conditions [45], H-theorem [38, 43]) and a number of numerical studies [42]. However, the complete regularized 13-moment equations have been derived only for Maxwell molecules. In [44], it has been demonstrated by the example of plane shock structure that the equations derived for Maxwell molecules are not directly applicable to the hard-sphere model, which indicates that collision models need to be taken into account during the model derivation. This inspires us to go beyond Maxwell molecules, and study more realistic interaction models directly. In this work, we will focus on inverse power potentials, which cover both Maxwell molecules and hard-sphere molecules (as the limit), and have been verified by experiments to be realistic for a number of gases [41, Table 8.1].

As far as we know, the only regularized moment model derived for non-Maxwell monatomic molecules is [37], which is the fully linearized equations for hard-sphere molecules. Such a model cannot be applied in nonlinear regimes such as shock waves. In this work, we are going to extend the work [37] and write down equations for all inverse power law models linearized about the *local Maxwellian*. The long derivation of the R13 equations is done by our automated Mathematica code. In [20], the authors already used computer algebra systems to derive complicated moment equations, which turns out to be much more efficient than using pen and paper. Plane shock wave structures will be computed based on these 13-moment models to show better results than a simple alteration of the Maxwell model.

The rest of this paper is organized as follows. In Section 2, we first introduce the explicit expressions of the R13 moment equations, and then show the linear stability analysis. In Section 3, the derivation of the R13 moment equations is presented. Some numerical experiments verifying the capability of the R13 system are carried out in Section 4 and some concluding remarks are made in Section 5. A brief introduction to the Boltzmann equation, the expressions of the infinite moment equations and the concrete form of the right-hand side of the R13 equations are given in the appendices.

2 R13 moment equations for linearized IPL model

In this section, we are going to present the regularized 13-moment equations for the IPL model, followed by their linear stability and dispersion relations. Before that, we start from a quick review of some properties of the IPL model.

2.1 A brief review of the IPL model

The IPL model contains a class of potentials that are frequently studied in the gas kinetic theory (c.f. [3, 14, 21, 35]). It assumes that the potential between two molecules is proportional to an inverse power of the distance between them:

$$\varphi(r) = \frac{\kappa}{1-\eta} r^{1-\eta},$$

where κ specifies the intensity of the force between particles. Based on this assumption, the viscosity coefficient of the gas in equilibrium is proportional to a certain power of the temperature of the gas, which is usually written by $\mu_{\text{ref}}(\theta/\theta_{\text{ref}})^\omega$, where θ is the temperature represented in the unit of specific energy:

$$\theta = \frac{k_B T}{\mathbf{m}}$$

with T being the temperature in Kelvin and k_B being the Boltzmann constant, and μ_{ref} is the reference viscosity coefficient at temperature θ_{ref} . The notation \mathbf{m} is the mass of a single molecule, and the viscosity index ω is related to η by $\omega = (\eta + 3)/(2\eta - 2)$. When $\eta = 5$, the model is Maxwell molecules, whose viscosity index is 1; when $\eta \rightarrow \infty$, the IPL model reduces to the hard-sphere model, whose viscosity index is 1/2. Detailed introduction to the IPL model based on kinetic models is presented in Appendix A.

Below we use the symbol μ to denote a more familiar “first approximation” of the viscosity coefficient, which is obtained by the truncated series expansion using Sonine polynomials [47]. For IPL models, the value of μ can be obtained by the following formula [3]:

$$\mu = \frac{5\mathbf{m}(k_B T/(\mathbf{m}\pi))^{1/2}(2k_B T/\kappa)^{2/(\eta-1)}}{8A_2(\eta)\Gamma[4-2/(\eta-1)]}, \quad (2.1)$$

with $A_2(\eta)$ being a constant depending only on η . Some of the values of this constant are given in Table 1.

η	5	7	10	17	∞
$A_2(\eta)$	0.4362	0.3568	0.3235	0.3079	0.3333

Table 1: Coefficients $A_2(\eta)$ for different η .

2.2 R13 moment equations

As the main result of this paper, the R13 moment equations for general IPL models will be presented in this section. For convenience, the equations are to be written down using “primitive variables”, which are density ρ , velocity v_i , temperature θ , tracefree stress tensor σ_{ij} , and heat flux q_i . All the indices run from 1 to 3. Due to the constraint $\sigma_{11} + \sigma_{22} + \sigma_{33} = 0$, these variables amount to 13 quantities as in Grad [18]. Below we are going to use the Einstein summation convention without using superscripts. For instance, the above constraint will be written as $\sigma_{ii} = 0$.

With these 13 variables, the equations for ρ , v_i and θ can be written by

$$\begin{aligned} \frac{d\rho}{dt} + \rho \frac{\partial v_k}{\partial x_k} &= 0, \\ \rho \frac{dv_i}{dt} + \theta \frac{\partial \rho}{\partial x_i} + \rho \frac{\partial \theta}{\partial x_i} + \frac{\partial \sigma_{ik}}{\partial x_k} &= 0, \\ \frac{3}{2}\rho \frac{d\theta}{dt} + \rho \theta \frac{\partial v_k}{\partial x_k} + \frac{\partial q_k}{\partial x_k} + \sigma_{kl} \frac{\partial v_k}{\partial x_l} &= 0, \end{aligned} \quad (2.2)$$

which are in fact the conservation laws of mass, momentum and total energy represented by primitive variables. More precisely, from the above equations, one can derive the equations for the momentum density ρv_i with momentum flux $\rho(v_i v_k + \theta \delta_{ik}) + \sigma_{ik}$, and for the energy density $\frac{1}{2}\rho(v_i v_i + 3\theta)$ with energy flux $\frac{1}{2}\rho v_k(v_i v_i + 5\theta) + \sigma_{ik} v_i + q_k$. To close the above system, the evolution of the stress tensor σ_{kl} and the heat flux q_k needs to be specified. The system (2.2) turns out to be Euler equations if σ_{ik} and q_k are set to be zero. Finer models based on Chapman-Enskog expansion, such as Navier-Stokes-Fourier equations, Burnett equations and super-Burnett equations, represent σ_{ik} and q_k using derivatives of ρ , v_i and θ . Following Grad [18], the 13-moment equations describe the evolution of σ_{ik} and q_k by supplementing (2.2) with additional equations. Here we adopt the form used in [35, eqs. (6.5)(6.6)] and write down these equations as:¹

$$\begin{aligned} & \frac{d\sigma_{ij}}{dt} + \sigma_{ij} \frac{\partial v_k}{\partial x_k} + \frac{4}{5} \frac{\partial q_{\langle i}}{\partial x_{j\rangle}} + 2\rho\theta \frac{\partial v_{\langle i}}{\partial x_{j\rangle}} + 2\sigma_{k\langle i} \frac{\partial v_{j\rangle}}{\partial x_k} + \frac{\partial m_{ijk}^{(\eta)}}{\partial x_k} = \Sigma_{ij}^{(\eta,1)} + \Sigma_{ij}^{(\eta,2)}, \\ & \frac{dq_i}{dt} + \frac{5}{2}\rho\theta \frac{\partial \theta}{\partial x_i} + \frac{5}{2}\sigma_{ik} \frac{\partial \theta}{\partial x_k} + \theta \frac{\partial \sigma_{ik}}{\partial x_k} - \theta \sigma_{ik} \frac{\partial \ln \rho}{\partial x_k} + \frac{7}{5}q_k \frac{\partial v_i}{\partial x_k} + \frac{2}{5}q_k \frac{\partial v_k}{\partial x_i} + \frac{7}{5}q_i \frac{\partial v_k}{\partial x_k} - \frac{\sigma_{ij}}{\rho} \frac{\partial \sigma_{jk}}{\partial x_k} \\ & + C^{(\eta)} \left(\sigma_{ik} \frac{\partial \theta}{\partial x_k} + \theta \frac{\partial \sigma_{ik}}{\partial x_k} \right) + \frac{1}{2} \frac{\partial R_{ijk}^{(\eta)}}{\partial x_k} + \frac{1}{6} \frac{\partial \Delta^{(\eta)}}{\partial x_i} + m_{ijk}^{(\eta)} \frac{\partial v_j}{\partial x_k} = Q_i^{(\eta,1)} + Q_i^{(\eta,2)}, \end{aligned} \quad (2.3)$$

where the angular brackets represent the symmetric and tracefree part of a tensor ($T_{\langle ij\rangle} = \frac{1}{2}(T_{ij} + T_{ji}) - \frac{1}{3}\delta_{ij}T_{kk}$ for any two-tensor T), and some values of the constant $C^{(\eta)}$ are listed in Table 2. In (2.3), the newly introduced variables $m_{ijk}^{(\eta)}$, $R_{ik}^{(\eta)}$ and $\Delta^{(\eta)}$ are the moments contributing to second- and higher-order terms in the Chapman-Enskog expansion,² and the right-hand sides $\Sigma_{ij}^{(\eta,1)}$, $\Sigma_{ij}^{(\eta,2)}$ and $Q_i^{(\eta,1)}$, $Q_i^{(\eta,2)}$ come from the collision between gas molecules. Here we assume that the collision is linearized about the local Maxwellian. Up to now, the system is exact but still not closed. The main contribution of this work is to close the system by providing expressions of $m_{ijk}^{(\eta)}$, $R_{ik}^{(\eta)}$, $\Delta^{(\eta)}$ and the right-hand sides using the 13 moments. Note that the moments $m_{ijk}^{(\eta)}$, $R_{ik}^{(\eta)}$, $\Delta^{(\eta)}$ are quantities appearing in Grad's 26-moment theory. More specifically, $m_{ijk}^{(\eta)}$ is the three-tensor formed by all tracefree third-order moments, and $R_{ik}^{(\eta)}$ and $\Delta^{(\eta)}$ are fourth-order moments. Below we first provide the expressions for $\Sigma_{ij}^{(\eta,1)}$ and $Q_i^{(\eta,1)}$:

$$\begin{aligned} \Sigma_{ij}^{(\eta,1)} &= D_0^{(\eta)} \frac{\theta \rho}{\mu} \sigma_{ij} + D_1^{(\eta)} \left(\frac{\partial v_{\langle i}}{\partial x_k} \sigma_{j\rangle k} + \frac{\partial v_k}{\partial x_{\langle i}} \sigma_{j\rangle k} \right) + D_2^{(\eta)} \frac{\partial v_k}{\partial x_k} \sigma_{ij} + D_3^{(\eta)} \rho \theta \frac{\partial v_{\langle i}}{\partial x_{j\rangle}}, \\ &+ D_4^{(\eta)} q_{\langle i} \frac{\partial \ln \theta}{\partial x_{j\rangle}} + D_5^{(\eta)} q_{\langle i} \frac{\partial \ln \rho}{\partial x_{j\rangle}} + D_6^{(\eta)} \frac{\partial q_{\langle i}}{\partial x_{j\rangle}}, \\ Q_i^{(\eta,1)} &= E_0^{(\eta)} \frac{\theta \rho}{\mu} q_i + E_1^{(\eta)} \sigma_{ik} \frac{\partial \theta}{\partial x_k} + E_2^{(\eta)} \theta \sigma_{ik} \frac{\partial \ln \rho}{\partial x_k} + E_3^{(\eta)} q_k \left(\frac{\partial v_k}{\partial x_i} + \frac{\partial v_i}{\partial x_k} \right) \\ &+ E_4^{(\eta)} q_i \frac{\partial v_k}{\partial x_k} + E_5^{(\eta)} \theta \frac{\partial \sigma_{ki}}{\partial x_k} + E_6^{(\eta)} \theta \rho \frac{\partial \theta}{\partial x_i}, \end{aligned} \quad (2.4)$$

¹In [35, eqs. (6.5)(6.6)], the author uses the notations u_{ijk}^0 , u_{ik}^1 and w^2 , while we use the notations $m_{ijk}^{(\eta)}$, $R_{ij}^{(\eta)}$ and $\Delta^{(\eta)}$. The relations are

$$m_{ijk}^{(\eta)} = u_{ijk}^0, \quad R_{ij}^{(\eta)} = u_{ij}^1 - (7 + 2C^{(\eta)})\theta \sigma_{ij}, \quad \Delta^{(\eta)} = w^2.$$

²This holds for any molecule potentials. We refer the readers to [35, eq. (8,14)], where our $R_{ij}^{(\eta)}$ is denoted by w_{ij}^1 .

where the coefficients $D_i^{(\eta)}$ and $E_i^{(\eta)}$ are partially tabulated in Table 3. Note that we have intentionally split the right-hand sides in (2.3) into two parts, so that the “generalized Grad 13-moment (GG13) equations” can be extracted from (2.3) by setting

$$m_{ijk}^{(\eta)} = R_{ik}^{(\eta)} = \Delta^{(\eta)} = \Sigma_{ij}^{(\eta,2)} = Q_i^{(\eta,2)} = 0. \quad (2.5)$$

The GG13 equations are introduced [34] by the order of magnitude method, and its fully linearized version for hard spheres has been derived in [37].

η	5	7	10	17	∞
$C^{(\eta)}$	0	-0.0715	-0.1193	-0.1615	-0.2161

Table 2: Coefficients $C^{(\eta)}$ for different η .

To give the R13 equations, we need to close (2.3) by specifying $m_{ijk}^{(\eta)}$, $R_{ik}^{(\eta)}$, $\Delta^{(\eta)}$, $\Sigma_{ij}^{(\eta,2)}$, and $Q_i^{(\eta,2)}$. The closure depends on the specific form of the collision model. Here we again assume that the collision is linearized about the local Maxwellian. Thus the R13 theory gives the following closure:

$$\begin{aligned} m_{ijk}^{(\eta)} &= \frac{\mu}{\theta\rho} \left(A_1^{(\eta)} q_{\langle i} \frac{\partial v_j}{\partial x_k} + A_2^{(\eta)} \theta \sigma_{\langle ij} \frac{\partial \ln \rho}{\partial x_k} + A_3^{(\eta)} \sigma_{\langle ij} \frac{\partial \theta}{\partial x_k} + A_4^{(\eta)} \theta \frac{\partial \sigma_{\langle ij}}{\partial x_k} \right), \\ \Delta^{(\eta)} &= \frac{\mu}{\theta\rho} \left(B_1^{(\eta)} \theta \frac{\partial q_k}{\partial x_k} + B_2^{(\eta)} \theta \sigma_{ij} \frac{\partial v_i}{\partial x_j} + B_3^{(\eta)} q_k \frac{\partial \theta}{\partial x_k} + B_4^{(\eta)} \theta q_k \frac{\partial \ln \rho}{\partial x_k} \right), \\ R_{ij}^{(\eta)} &= C_0^{(\eta)} \theta \sigma_{ij} + \frac{\mu}{\theta\rho} \left(C_1^{(\eta)} \theta \frac{\partial q_{\langle i}}{\partial x_j} + C_2^{(\eta)} \theta \sigma_{k\langle i} \frac{\partial v_j}{\partial x_k} + C_3^{(\eta)} \theta^2 \rho \frac{\partial v_{\langle i}}{\partial x_j} + C_4^{(\eta)} q_{\langle i} \frac{\partial \theta}{\partial x_j} + C_5^{(\eta)} \theta q_{\langle i} \frac{\partial \ln \rho}{\partial x_j} \right). \end{aligned} \quad (2.6)$$

Some values of the coefficients $A_i^{(\eta)}$, $B_i^{(\eta)}$, and $C_i^{(\eta)}$ are given in Table 3. The full expressions of $\Sigma_{ij}^{(\eta,2)}$ and $Q_i^{(\eta,2)}$ are quite lengthy and we provide them in Appendix C. A simple case is $\eta = 5$, for which we have

$$\Sigma_{ij}^{(5,2)} = 0, \quad Q_i^{(5,2)} = 0, \quad (2.7)$$

and the corresponding model matches the one derived for Maxwell molecules in [36] (with terms nonlinear in σ_{ij} and q_i removed since we use the linearized collision model).

2.3 Discussion on the order of accuracy

One possible way to describe the accuracy of the moment models in the near-continuum regime is to use the notion of “order of accuracy” [34, 35]. In such a regime, the Knudsen number Kn , i.e. the ratio of the mean free path to the characteristic length of the problem, is regarded as a small number. Thus Chapman-Enskog expansion can be applied, and all non-equilibrium moments are expanded into power series of Kn , e.g.,

$$\begin{aligned} \sigma_{ij} &= Kn \sigma_{ij}^{(1)} + Kn^2 \sigma_{ij}^{(2)} + Kn^3 \sigma_{ij}^{(3)} + \dots, \\ q_i &= Kn q_i^{(1)} + Kn^2 q_i^{(2)} + Kn^3 q_i^{(3)} + \dots. \end{aligned} \quad (2.8)$$

By asymptotic analysis, all these terms can be represented by the conservative variables and their derivatives. Truncating the above series up to the term Kn^k and inserting the result into (2.2), one obtains moment equations with k th order of accuracy. By this approach, the models derived from Chapman-Enskog expansion up to zeroth to third order are, respectively, Euler

η		0	1	2	3	4	5	6
5	$A_i^{(\eta)}$	×	-1.6	2	0	-2	×	×
	$B_i^{(\eta)}$	×	-12	-12	-30	12	×	×
	$C_i^{(\eta)}$	0	-4.8	-6.8571	0	-4.8	4.8	×
	$D_i^{(\eta)}$	-1.0	0	0	0	0	0	0
	$E_i^{(\eta)}$	-0.6667	0	0	0	0	0	0
7	$A_i^{(\eta)}$	×	-1.4430	2.0094	0.2417	-1.9679	×	×
	$B_i^{(\eta)}$	×	-11.4061	-11.2200	-27.5608	12.0836	×	×
	$C_i^{(\eta)}$	-0.1226	-4.7155	-6.6789	-0.2456	-3.7894	4.7705	×
	$D_i^{(\eta)}$	-0.9967	0.0404	-0.0269	0.0030	0.0254	-0.0576	0.0569
	$E_i^{(\eta)}$	-0.6636	0.1075	0.0005	0.0441	-0.0294	0.0	0.0046
10	$A_i^{(\eta)}$	×	-1.3445	2.0266	0.40152	-1.9562	×	×
	$B_i^{(\eta)}$	×	-11.0838	-10.7755	-26.1567	12.2346	×	×
	$C_i^{(\eta)}$	-0.2051	-4.6797	-6.5941	-0.4122	-3.1530	4.7727	×
	$D_i^{(\eta)}$	-0.9909	0.0669	-0.0446	0.0085	0.0347	-0.0967	0.0948
	$E_i^{(\eta)}$	-0.6582	0.1757	0.0015	0.0733	-0.0489	-0.0001	0.0129
17	$A_i^{(\eta)}$	×	-1.2609	2.0493	0.5429	-1.9523	×	×
	$B_i^{(\eta)}$	×	-10.8444	-10.4280	-25.0494	12.4328	×	×
	$C_i^{(\eta)}$	-0.2784	-4.6617	-6.5415	-0.5618	-2.6123	4.7895	×
	$D_i^{(\eta)}$	-0.9834	0.0900	-0.0600	0.0156	0.0379	-0.1316	0.1279
	$E_i^{(\eta)}$	-0.6512	0.2332	0.0028	0.0987	-0.0658	-0.0002	0.0237
∞	$A_i^{(\eta)}$	×	-1.1542	2.0902	0.7315	-1.9562	×	×
	$B_i^{(\eta)}$	×	-10.5892	-10.0287	-23.7646	12.7856	×	×
	$C_i^{(\eta)}$	-0.3749	-4.6572	-6.5039	-0.7619	-1.9262	4.8328	×
	$D_i^{(\eta)}$	-0.9703	0.1195	-0.0797	0.0282	0.0347	-0.1773	0.1707
	$E_i^{(\eta)}$	-0.6392	0.3049	0.0052	0.1313	-0.0875	-0.0003	0.0427

Table 3: Coefficient of $A_i^{(\eta)}$, $B_i^{(\eta)}$, $C_i^{(\eta)}$, $D_i^{(\eta)}$ and $E_i^{(\eta)}$ for different η .

equations, Navier-Stokes-Fourier equations, Burnett equations, and super-Burnett equations. These equations contain only equilibrium variables: density, velocity and temperature.

In the 13-moment model, one can also assume Kn is small and apply the expansion (2.8) to obtain models including only equilibrium variables. Suppose the second-order Chapman-Enskog expansion of a moment model agrees with the Burnett equations, while its third-order Chapman-Enskog expansion differs from super-Burnett equations, then we say that the moment model has the second-order accuracy (or Burnett order). For example, Grad's 13-moment equations have the first-order accuracy for general IPL potentials, but have second-order accuracy for Maxwell molecules; GG13 equations are extensions to Grad's 13-moment theory to achieve second-order accuracy for all molecule potentials. In general, the expansion (2.8) is usually obtained by multiplying the equations of σ_{ij} and q_i in the moment system by Kn . Therefore in most cases, a 13-moment model has k th-order accuracy if the equations for σ_{ij} and q_i (2.3) are accurate up to the $(k-1)$ th order. R13 equations have the third-order accuracy, as the closure (2.6) provides the equations (2.3) exact second-order contributions.

In the literature, there exist some similar 13-moment models obtained by other approaches to include second-order derivatives in the equations for σ_{ij} and q_i . For instance, the relaxed Burnett equations [23] are also derived for arbitrary interaction potentials, and as mentioned in [23, 35], these equations have second-order accuracy. Another similar model is the NCCR (Nonlinear Coupled Constitutive Relations) equations [31]. These equations do not include information from the Burnett order, and therefore they have the first-order accuracy and distinguish different

interaction models by viscosity and heat conductivity coefficients. The full R13 models for Maxwell molecules and the BGK model, which have the third-order accuracy, have been derived in [36] and [35], and the linear R13 equations for the hard-sphere model have been derived in [37].

2.4 Linear stability and dispersion

For the newly proposed R13 equations for IPL models, we are going to check some of its basic properties in this work. In this section, we focus on the linear properties including its stability in time and space, and the dispersion and damping of sound waves.

Following [36, 35, 37], we apply the analysis to one-dimensional linear dimensionless equations. The linearization is performed about a global equilibrium state with density ρ_0 , zero velocity, and temperature θ_0 . The derivation of the one-dimensional linear dimensionless equations consists of the following steps:

1. Introduce the *small* dimensionless variables $\hat{\rho}$, $\hat{\theta}$, \hat{v}_i , $\hat{\sigma}_{ij}$, and \hat{q}_i by

$$\rho = \rho_0(1 + \hat{\rho}), \quad \theta = \theta_0(1 + \hat{\theta}), \quad v_i = \sqrt{\theta_0}\hat{v}_i, \quad \sigma_{ij} = \rho_0\theta_0\hat{\sigma}_{ij}, \quad q_i = \rho_0\sqrt{\theta_0^3}\hat{q}_i. \quad (2.9)$$

2. Let L be the characteristic length, and define the dimensionless space and time variables by

$$x_i = L\hat{x}_i, \quad t = \frac{L}{\sqrt{\theta_0}}\hat{t}. \quad (2.10)$$

3. Substitute (2.9)(2.10) into the R13 equations (2.2)(2.3) and (2.6), and drop all the terms nonlinear in the variables with hats introduced in (2.9).
4. Reduce the resulting equations to the one-dimensional system by dropping all the terms with derivatives with respect to x_2 and x_3 , and setting

$$\begin{aligned} \hat{v}_1 = \hat{v}, \quad \hat{q}_1 = \hat{q}, \quad \hat{\sigma}_{11} = \hat{\sigma}, \quad \hat{\sigma}_{22} = \hat{\sigma}_{33} = -\frac{1}{2}\hat{\sigma}, \\ \hat{v}_2 = \hat{v}_3 = \hat{q}_2 = \hat{q}_3 = \hat{\sigma}_{12} = \hat{\sigma}_{23} = \hat{\sigma}_{13} = 0. \end{aligned} \quad (2.11)$$

The resulting equations can be written down more neatly if we introduce the Knudsen number

$$Kn = \frac{\mu_0\sqrt{\theta_0}}{\rho_0\theta_0 L}, \quad (2.12)$$

where μ_0 is the viscosity coefficient at temperature θ_0 . For all IPL models, the one-dimensional

linear dimensionless equations have the form:

$$\begin{aligned}
\frac{\partial \hat{\rho}}{\partial \hat{t}} + \frac{\partial \hat{v}}{\partial \hat{x}} &= 0, \\
\frac{\partial \hat{v}}{\partial \hat{t}} + \frac{\partial \hat{\theta}}{\partial \hat{x}} + \frac{\partial \hat{\rho}}{\partial \hat{x}} + \frac{\partial \hat{\sigma}}{\partial \hat{x}} &= 0, \\
\frac{\partial \hat{\theta}}{\partial \hat{t}} + \frac{2}{3} \frac{\partial \hat{q}}{\partial \hat{x}} + \frac{2}{3} \frac{\partial \hat{v}}{\partial \hat{x}} &= 0, \\
\frac{\partial \hat{\sigma}}{\partial \hat{t}} + \frac{8}{15} \frac{\partial \hat{q}}{\partial \hat{x}} + \frac{4}{3} \frac{\partial \hat{v}}{\partial \hat{x}} + \underline{\underline{Kn \alpha_1^{(\eta)} \frac{\partial^2 \hat{\sigma}}{\partial \hat{x}^2}}} &= \frac{\alpha_2^{(\eta)}}{Kn} \hat{\sigma} + \frac{\alpha_3^{(\eta)}}{Kn} \hat{\sigma} + \alpha_4^{(\eta)} \frac{\partial \hat{q}}{\partial \hat{x}} + \alpha_5^{(\eta)} \frac{\partial \hat{v}}{\partial \hat{x}} + \\
\underline{\underline{\frac{\alpha_6^{(\eta)}}{Kn} \hat{\sigma} + \alpha_7^{(\eta)} \frac{\partial \hat{q}}{\partial \hat{x}} + \alpha_8^{(\eta)} \frac{\partial \hat{v}}{\partial \hat{x}} + Kn \left(\alpha_9^{(\eta)} \frac{\partial^2 \hat{\theta}}{\partial \hat{x}^2} + \alpha_{10}^{(\eta)} \frac{\partial^2 \hat{\rho}}{\partial \hat{x}^2} + \alpha_{11}^{(\eta)} \frac{\partial^2 \hat{\sigma}}{\partial \hat{x}^2} \right)}}, & \\
\frac{\partial \hat{q}}{\partial \hat{t}} + \beta_1^{(\eta)} \frac{\partial \hat{\sigma}}{\partial \hat{x}} + \frac{5}{2} \frac{\partial \hat{\theta}}{\partial \hat{x}} + \underline{\underline{\beta_2^{(\eta)} \frac{\partial \hat{\sigma}}{\partial \hat{x}} + \beta_3^{(\eta)} Kn \frac{\partial^2 \hat{q}}{\partial \hat{x}^2} + \beta_4^{(\eta)} Kn \frac{\partial^2 \hat{v}}{\partial \hat{x}^2}}} &= \frac{\beta_5^{(\eta)}}{Kn} \hat{q} + \\
\underline{\underline{\frac{\beta_6^{(\eta)}}{Kn} \hat{q} + \beta_7^{(\eta)} \frac{\partial \hat{\theta}}{\partial \hat{x}} + \beta_8^{(\eta)} \frac{\partial \hat{\sigma}}{\partial \hat{x}} + \frac{\beta_9^{(\eta)}}{Kn} \hat{q} + \beta_{10}^{(\eta)} \frac{\partial \hat{\theta}}{\partial \hat{x}} + \beta_{11}^{(\eta)} \frac{\partial \hat{\sigma}}{\partial \hat{x}} + Kn \left(\beta_{12}^{(\eta)} \frac{\partial^2 \hat{q}}{\partial \hat{x}^2} + \beta_{13}^{(\eta)} \frac{\partial^2 \hat{v}}{\partial \hat{x}^2} \right)}}, &
\end{aligned} \tag{2.13}$$

where $\alpha_i^{(\eta)}$ and $\beta_i^{(\eta)}$ depend only on η , and their values for some choices of η are listed in Table 4. In (2.13), if we replace all the terms with double underlines by zero, we obtain the linearized GG13 equations. Furthermore, if we set all the terms with both single and double underlines to be zero, then the result is the linearized Navier-Stokes-Fourier equations. The left-hand side of (2.13) comes from the advection, and the right-hand side comes from the collision. By Table 4, it can be clearly seen that when $\eta = 5$ (Maxwell molecules), due to the simplicity of the collision operator, all the underlined terms on the right-hand side disappear.

For simplicity, we will omit the hats on the variables hereafter. In general, the linear GG13 or R13 system has the form

$$\frac{\partial u_A}{\partial t} + \mathcal{A}_1^{(\eta)} \frac{\partial u_A}{\partial x} + \mathcal{A}_2^{(\eta)} \frac{\partial^2 u_A}{\partial x^2} + \mathcal{A}_3^{(\eta)} u_A = 0, \tag{2.14}$$

where $u_A = (\rho, v, \theta, \sigma, q)^T$ and the matrices $\mathcal{A}_i^{(\eta)}$ are constant matrices which can be observed from (2.13). To study the linear waves, we consider the plane wave solution:

$$u_A(x, t) = \tilde{u}_A \exp[i(\Omega t - kx)], \tag{2.15}$$

where \tilde{u}_A is the initial amplitude of the wave, Ω is frequency and k is the wave number. Inserting the above solution into (2.14) yields

$$\mathcal{G}^{(\eta)} \tilde{u}_A = 0, \quad \text{where} \quad \mathcal{G}^{(\eta)} = \left(i\Omega - ik\mathcal{A}_1^{(\eta)} - k^2\mathcal{A}_2^{(\eta)} + \mathcal{A}_3^{(\eta)} \right). \tag{2.16}$$

and the existence of nontrivial solutions requires

$$\det[\mathcal{G}^{(\eta)}] = 0. \tag{2.17}$$

From (2.17), we can get the relation between Ω and k , and thus all the desired properties such as the amplification and dispersion of the linear waves can naturally be obtained. In our analysis below, we choose $Kn = 1$ to get quantitative results.

η		1	2	3	4	5	6	7
5	$\alpha_i^{(\eta)}$	-1.2	-1	0	0	0	0	0
	$\beta_i^{(\eta)}$	1	0	-3.6	0	-2/3	0	0
7	$\alpha_i^{(\eta)}$	-1.1808	-0.9983	0.0015	0.0380	0.0020	0.0013	0.0217
	$\beta_i^{(\eta)}$	0.9285	-0.0613	-3.4729	-0.0819	-0.6648	0.0012	0.0046
10	$\alpha_i^{(\eta)}$	-1.1737	-0.9951	0.0042	0.0632	0.0056	0.0037	0.0362
	$\beta_i^{(\eta)}$	0.8806	-0.1026	-3.4072	-0.1374	-0.6616	0.0034	0.0129
17	$\alpha_i^{(\eta)}$	-1.1714	-0.9911	0.0077	0.0853	0.0104	0.0068	0.0490
	$\beta_i^{(\eta)}$	0.8385	-0.1392	-3.3613	-0.1873	-0.6574	0.0062	0.0237
∞	$\alpha_i^{(\eta)}$	-1.1737	-0.9842	0.0139	0.1138	0.0188	0.0124	0.0659
	$\beta_i^{(\eta)}$	0.7839	-0.1875	-3.3173	-0.2540	-0.6503	0.0111	0.0427
η		8	9	10	11	12	13	
5	$\alpha_i^{(\eta)}$	0	0	0	0	×	×	
	$\beta_i^{(\eta)}$	0	0	0	0	0	0	
7	$\alpha_i^{(\eta)}$	0.0017	0.0809	0.0017	0.0105	×	×	
	$\beta_i^{(\eta)}$	0.0	0.0008	0.0031	-0.0003	-0.1440	0.0011	
10	$\alpha_i^{(\eta)}$	0.0049	0.1352	0.0050	0.0202	×	×	
	$\beta_i^{(\eta)}$	-0.0001	0.0023	0.0087	-0.0008	-0.2225	0.0036	
17	$\alpha_i^{(\eta)}$	0.0091	0.1840	0.0093	0.0308	×	×	
	$\beta_i^{(\eta)}$	-0.0002	0.0042	0.0161	-0.0012	-0.2814	0.0076	
∞	$\alpha_i^{(\eta)}$	0.0168	0.2499	0.0173	0.0476	×	×	
	$\beta_i^{(\eta)}$	-0.0003	0.0077	0.0295	-0.0015	-0.3451	0.0160	

Table 4: Coefficients of the linearized R13 system for different η .

Remark 1. The equations (2.13) in the case $\eta = \infty$ can be used to compare with the results in [37] for cross-checking. Small deviation between our coefficients and the coefficients in [37] can be observed. For example, in [37], the value of $\alpha_2^{(\infty)}$ is -0.98632 , while our analysis gives $\alpha_2^{(\infty)} = -0.9842$. We believe that such discrepancies are due to different truncation when inverting the collision operator during the derivation. According to the method reported in [37, eq. (23)], our result is probably more accurate since we preserve more terms in the truncation. Details are to be given in Section 3.

2.4.1 Linear stability in time and space

We first discuss the linear stability of the generalized G13 and R13 systems in time and space. For the time stability, we require that the norm of the amplitude decreases with time for any given wave number $k \in \mathbb{R}$. Precisely, if we assume $\Omega = \Omega_r(k) + i\Omega_i(k)$, the time stability requires $\Omega_i(k) \geq 0$. Figure 1 shows possible values of $\Omega_i(k)$ on the complex plane. Note that $\Omega_i(k)$ is a multi-valued function since (2.17) may have multiple solutions for a given k . It is observed that for all choices η , the values of $\Omega(k)$ always locate on the upper half of the complex plane, indicating the linear stability for both R13 and generalized G13 equations.

For the stability in space, we require that for a given wave frequency, the amplitude should not increase along the direction of wave propagation. Now we assume that $\Omega \in \mathbb{R}$ is given, and let $k = k_r(\Omega) + ik_i(\Omega)$. Then the wave is stable in space if $k_r(\Omega)k_i(\Omega) \leq 0$. Figure 2 shows the values of k on the complex plane with Ω as the parameter. The results show that all the curves do not enter the upper right or the lower left quadrant for both R13 and generalized G13 equations, showing the spatial stability for both models. Again, such a stability result holds for all η considered in our experiments.

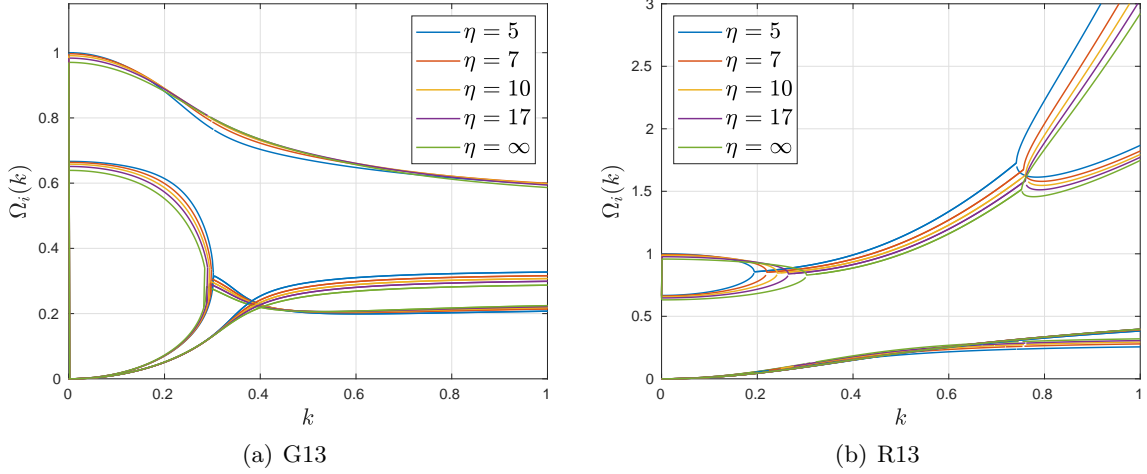


Figure 1: Damping coefficients $\Omega_i(k)$ of the G13 and R13 systems for different η .

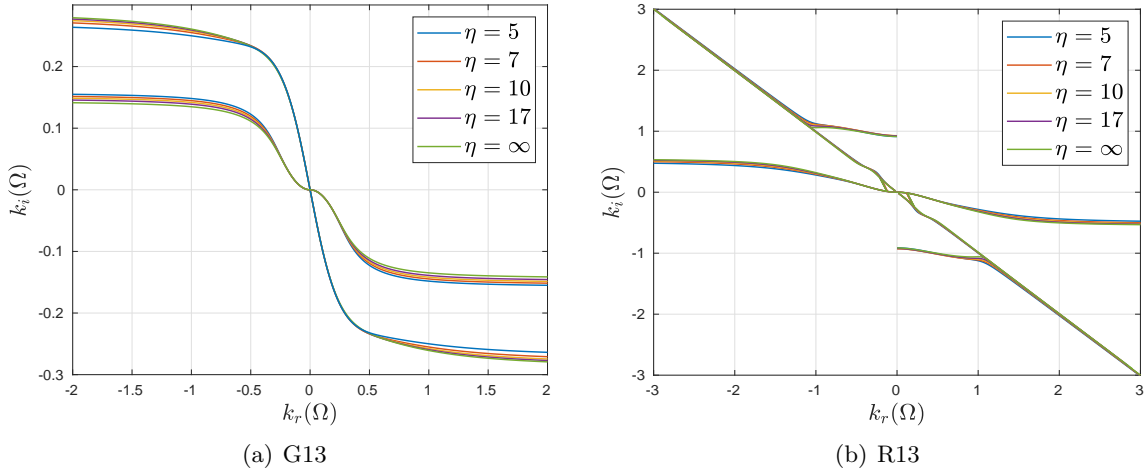


Figure 2: The solutions $k(\Omega)$ of the dispersion relation in the complex plane with Ω as parameter of the G13 and R13 systems for different η .

2.4.2 Dispersion and damping

We proceed by discussing the phase speeds as functions of frequency for the R13 and GG13 systems. For a given wave frequency Ω , we define the damping rate α and the wave speed v_{ph} by

$$\alpha = -k_i(\Omega), \quad v_{ph} = \frac{\Omega}{k_r(\Omega)}. \quad (2.18)$$

For the Euler equations, where $\sigma = q = 0$ in (2.13), the absolute phase velocity is $|v_{ph}| = \sqrt{5/3}$ for all wave frequency Ω . For R13 and GG13 equations, v_{ph} depends on Ω , causing the dispersion of sound waves. Here we define the dimensionless phase speed $c_{ph} = v_{ph}/\sqrt{5/3}$ and plot c_{ph} as a function of the frequency Ω in Figure 3 for R13 and GG13 equations. Note that $c_{ph}(\Omega)$ is also a multi-valued function, and in Figure 3, we only plot the positive phase velocities. For GG13 equations, the phase velocity has an upper limit, indicating the hyperbolic nature of the system, while R13 equations can achieve infinitely large phase velocities. In general, the phase speeds do not change much as η varies, which predicts similar behavior of sound waves in different

monatomic gases.

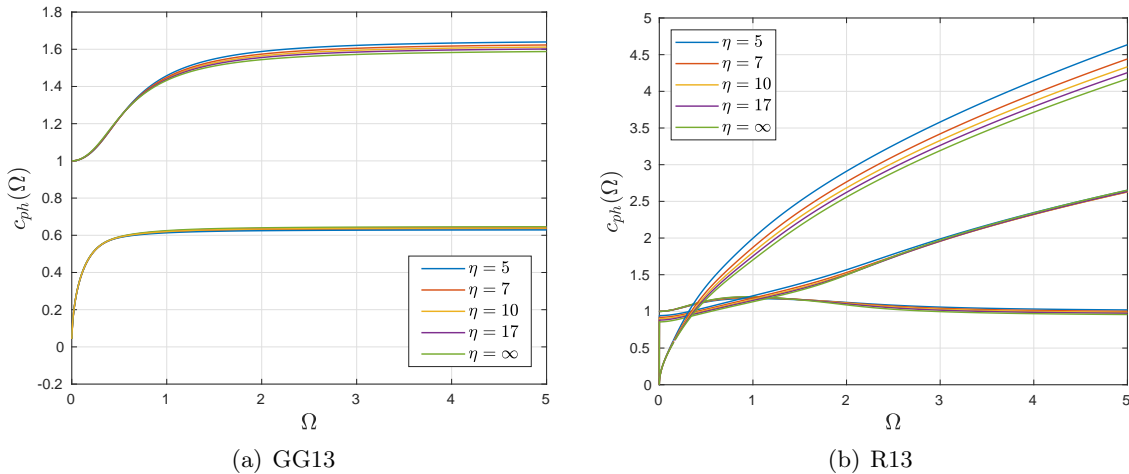


Figure 3: Phase speed c_{ph} over frequency Ω of the G13 and R13 systems for different η .

To study the phase speeds for large frequency waves, we plot the inverse wave speed $1/c_{ph}$ as a function of the inverse frequency $1/\Omega$ in Figure 4(a), and the reduced damping rate α/Ω is plotted in Figure 4(b) also as a function of $1/\Omega$. In these figures, only the mode with the weakest damping is given. Figure 4(a) shows that for GG13 equations, the phase velocity increases monotonically as the frequency increases, while for R13 equations, the wave slows down as Ω reaches a value close to 1. Such an observation agrees with the results in [36, 37], while the experimental results for argon [28] suggest the monotonicity of the phase velocity, which is closer to the prediction of GG13 equations. Note that here we set the Knudsen number Kn to be 1. For another Knudsen number, the actual frequency of the wave should be Ω/Kn . This means that if we consider a wave with a fixed actual frequency travelling in the gas with a low Knudsen number, we need to focus on large values of Ω^{-1} . Indeed, when $\Omega^{-1} > 1$, R13 models give better approximation of the phase velocity, while for small Ω^{-1} , which corresponds to large Knudsen numbers, there is no guarantee whether R13 or GG13 is superior, and the reason why GG13 provides better prediction requires further investigation. Nevertheless, for the damping rate shown in Figure 4(b), R13 equations give significantly better agreement with the experimental data for the whole range of the frequency.

3 Derivation of moment systems

In this section, we provide the detailed procedure to derive GG13 and R13 equations. In general, both models can be derived from infinite moment equations by the method of order of magnitude. Following [18], the moments can be considered as the coefficients in the series expansion of the distribution function in the gas kinetic theory. The distribution function is a function of position \mathbf{x} , particle velocity $\boldsymbol{\xi}$, and time t , which is a mesoscopic description of fluid states in statistical physics. The moment method proposed by Grad [18] is one of the methods to derive macroscopic models from the kinetic theory. Our starting point is the same as [18], but we adopt the form used in [24], which expands the distribution function $f(\mathbf{x}, \boldsymbol{\xi}, t)$ as

$$f(\mathbf{x}, \boldsymbol{\xi}, t) = \sum_{l=0}^{+\infty} \sum_{m=-l}^l \sum_{n=0}^{+\infty} f_{lmn}(\mathbf{x}, t) \psi_{lmn}(\mathbf{x}, \boldsymbol{\xi}, t), \quad (3.1)$$

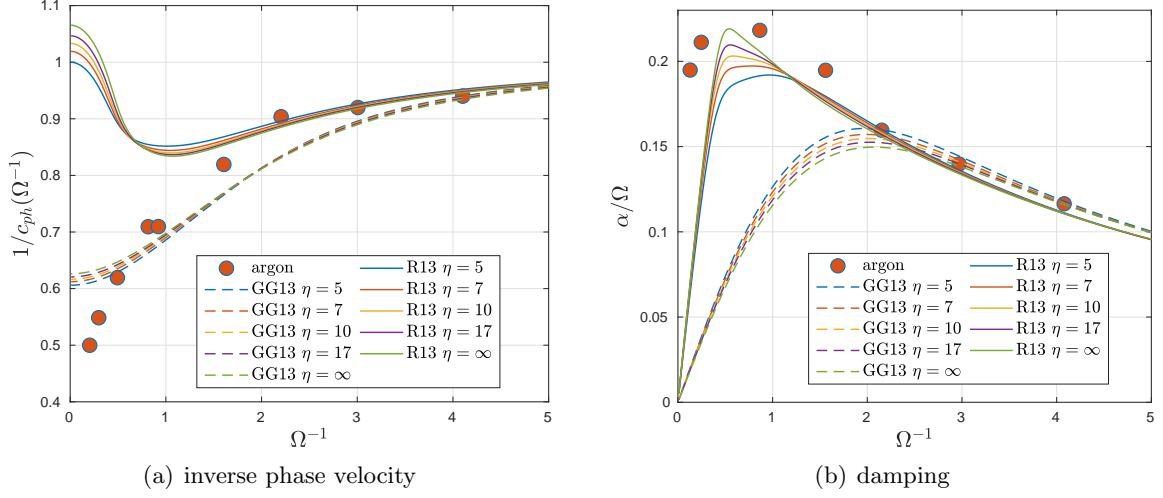


Figure 4: Inverse phase speed and damping over frequency Ω of the G13 and R13 systems for different η . The bullets are the experimental results for argon [28].

where $\psi_{lmn}(\cdot)$ is the basis function based on Sonine polynomials and spherical harmonics, the detailed form of which is listed in Appendix B. Here $\mathbf{v} = (v_1, v_2, v_3)^T$ is the velocity vector. The coefficients f_{lmn} satisfy $\overline{f_{lmn}} = (-1)^m f_{l,-m,n}$, and they are related to Grad's 13 moments by

$$\begin{aligned}
f_{000} &= \rho, & f_{1m0} &= 0, & m &= -1, 0, 1, & f_{001} &= 0, \\
\sigma_{11} &= \sqrt{2}\text{Re}(f_{220}) - f_{200}/\sqrt{3}, & \sigma_{12} &= -\sqrt{2}\text{Im}(f_{220}), & \sigma_{13} &= -\sqrt{2}\text{Re}(f_{210}), \\
\sigma_{22} &= -\sqrt{2}\text{Re}(f_{220}) - f_{200}/\sqrt{3}, & \sigma_{23} &= \sqrt{2}\text{Im}(f_{210}), & \sigma_{33} &= 2f_{200}/\sqrt{3}, \\
q_1 &= \sqrt{5}\text{Re}(f_{111}), & q_2 &= -\sqrt{5}\text{Im}(f_{111}), & q_3 &= -\sqrt{5/2}f_{101}.
\end{aligned} \tag{3.2}$$

These relations indicate the equivalence between Grad's 13-moments and the following 13 variables:

$$f_{000}, v_1, v_2, v_3, \theta, f_{220}, f_{210}, f_{200}, f_{2,-1,0}, f_{2,-2,0}, f_{111}, f_{101}, f_{1,-1,1}. \tag{3.3}$$

Below we focus only on the derivation of equations for these quantities.

The exact evolution equations for f_{lmn} have been derived from the Boltzmann equation with linearized collision operator in [12]. In general, the equations for other f_{lmn} have the form

$$\frac{\partial f_{lmn}}{\partial t} + S_{lmn} + T_{lmn} = \frac{\rho\theta}{\mu} \sum_{n'=0}^{+\infty} a_{lnn'} \theta^{n-n'} f_{lmn'}, \tag{3.4}$$

where S_{lmn} contains time derivatives and T_{lmn} contains spatial derivatives. More precisely, S_{lmn} is the linear combination of the terms

$$\frac{\partial \theta}{\partial t} f_{l,m',n-1}, \quad \frac{\partial v_i}{\partial t} f_{l-1,m',n}, \quad \text{and} \quad \frac{\partial v_i}{\partial t} f_{l+1,m',n-1} \tag{3.5}$$

with $i = 1, 2, 3$ and $m' = m - 1, m, m + 1$, and T_{lmn} has the form

$$T_{lmn} = \sum_{l',m',n'} \left(\alpha_{lmn}^{l'm'n'} (\nabla_{\mathbf{x}} \mathbf{v}, \nabla_{\mathbf{x}} \theta, \mathbf{v}, \theta) f_{l'm'n'} + \sum_{i=1}^3 \beta_{lmn,i}^{l'm'n'}(\mathbf{v}, \theta) \frac{\partial f_{l'm'n'}}{\partial x_i} \right),$$

which shows that T_{lmn} is linear in all the coefficients $f_{l'm'n'}$, while the linear coefficients are nonlinear functions of \mathbf{v} , θ and their spatial derivatives. The convection term T_{lmn} also has the following properties:

(P1) The differential operator appears only once in each coefficient $\alpha_{lmn}^{l'm'n'}(\nabla_{\mathbf{x}}\mathbf{v}, \nabla_{\mathbf{x}}\theta, \mathbf{v}, \theta)$.

(P2) The coefficients $\alpha_{lmn}^{l'm'n'}(\nabla_{\mathbf{x}}\mathbf{v}, \nabla_{\mathbf{x}}\theta, \mathbf{v}, \theta)$ and $\beta_{lmn,i}^{l'm'n'}(\mathbf{v}, \theta)$ are nonzero only if

$$l + 2n - 3 \leq l' + 2n' \leq l + 2n + 1, \quad l - 2 \leq l' \quad \text{and} \quad n - 2 \leq n' \leq n + 1.$$

The second property (P2) will play an important role in the derivation of moment equations.

The precise expressions of S_{lmn} and T_{lmn} will be given in Appendix B, and on the right-hand side of (3.4), $a_{lmn'}$ are pure numbers for all IPL models. Note that (3.4) has already included the conservation laws (2.2), which can be obtained by setting (l, m, n) to be

$$(0, 0, 0), \quad (1, -1, 0), \quad (1, 0, 0), \quad (1, 1, 0), \quad (0, 0, 1).$$

The subsequent derivation may include tedious formulas, and in our implementation, all the calculations are done by the computer algebra system Wolfram Mathematica. Below we only describe the algorithm we use in the Mathematica code, and will not write out the lengthy intermediate results in the calculational process.

Remark 2. Note that complex basis functions ψ_{lmn} are introduced in the expansion (3.1), resulting in complex coefficients f_{lmn} , which seems to complicate the derivation. In Grad's original formulation [18], basis functions based on Cartesian coordinates are considered, so that all the coefficients are real. However, in Grad's original expansion using Hermite polynomials, one cannot find 13 coefficients which matches exactly all the moments in his 13-moment equations. Our basis functions, which are similar to the ones in [25], correspond to the 13 moments very well (see (3.3)). Meanwhile, our basis functions are based on spherical coordinates, so that the rotational invariance of the collision operator can be easily utilized to simplify the calculation. Based on spherical coordinates, complex basis functions can also be avoided by using real spherical harmonics instead of complex spherical harmonics [2, Section 1.5.2]. However, real spherical harmonics do not have simple recurrence formulas such as [1, Eqs. (15.150)(15.151)], which will result in a more complicated form of S_{lmn} and T_{lmn} .

3.1 General idea for the moment closure

Before providing the details of the derivation, we would first like to explain the general methodology of the moment closure. To close the advection term, one can observe from (2.3) that we need to provide expressions for the moments m_{ijk} , R_{ik} and Δ , which correspond to the coefficients f_{3m0} , f_{1m1} and f_{002} , respectively. To close the collision term, it can be seen from (3.4) that we have to provide expressions for infinite terms f_{1mn} and f_{2mn} for any positive integer n . In our implementation, this is done by a truncation of the infinite series in (3.4), whose fast convergence has already been demonstrated in [11], so that only a finite number of coefficients need to be considered.

The derivation of R13 equations is mostly similar to the Chapman-Enskog expansion. However, there are two key differences:

- (K1) All the moments are to be represented by the 13 moments and their derivatives, while only 5 equilibrium moments are involved in the Chapman-Enskog expansion;
- (K2) We expect that the equations have the Burnett order and involve only second-order derivatives, while third-order derivatives are involved in Burnett equations.

Due to the first difference, there are in principle infinite versions of R13 equations in the Burnett order, since the leading order terms in σ_{ij} and q_i can be represented by equilibrium variables:

$$\sigma_{ij} \approx -\frac{2\mu}{\alpha_2^{(\eta)}} \frac{\partial v_{\langle i}}{\partial x_{j\rangle}}, \quad q_i \approx -\frac{5\mu}{2\beta_5^{(\eta)}} \frac{\partial \theta}{\partial x_i}, \quad (3.6)$$

as already resulted in many different versions of R13 equations for Maxwell molecules [40]. In our derivation, since σ_{ij} and q_i are already included in the system, we will avoid using (3.6) to make any replacement except in the derivation of first-order expressions. More precisely, according to Chapman-Enskog expansion, the first-order term of the distribution function can be completely represented by the following quantities:

$$\rho, v_i, \theta, \frac{\partial v_{\langle i}}{\partial x_{j\rangle}}, \frac{\partial \theta}{\partial x_i}.$$

At this step, we will apply (3.6) to replace the derivatives of v_i and θ by σ_{ij} and q_i . By such replacement, one order of derivative can be eliminated, so that (K2) can be automatically achieved.

3.2 Chapman-Enskog expansion of the coefficients

This section is devoted to the details of the asymptotic analysis. As mentioned in the previous section, the idea of Chapman-Enskog expansion is utilized here to derive models with different orders of accuracy. To begin with, we introduce the scaling $t = t'/\epsilon$ and $x_i = x'_i/\epsilon$, and rewrite the equations (3.4) with time and spatial variables t' and x'_i . In the resulting equations, a factor ϵ^{-1} is introduced to the right-hand side of (3.4). In this section, we will work on the scaled equations, and the prime symbol on t' and x'_i will be omitted. Based on such a transform, we write down the asymptotic expansion for all the moments as

$$f_{lmn} = f_{lmn}^{(0)} + \epsilon f_{lmn}^{(1)} + \epsilon^2 f_{lmn}^{(2)} + \epsilon^3 f_{lmn}^{(3)} + \dots. \quad (3.7)$$

In the original Chapman-Enskog expansion of the distribution function $f = f^{(0)} + \epsilon f^{(1)}$, we require that $f^{(0)}$ is the local Maxwellian \mathcal{M} . The corresponding assumption for the coefficients is

$$f_{lmn}^{(0)} = \begin{cases} \rho, & \text{if } (l, m, n) = (0, 0, 0), \\ 0, & \text{otherwise,} \end{cases} \quad (3.8)$$

By (3.7), the term S_{lmn} and T_{lmn} can be expanded correspondingly:

$$S_{lmn} = S_{lmn}^{(0)} + \epsilon S_{lmn}^{(1)} + \epsilon^2 S_{lmn}^{(2)} + \epsilon^3 S_{lmn}^{(3)} + \dots, \quad T_{lmn} = T_{lmn}^{(0)} + \epsilon T_{lmn}^{(1)} + \epsilon^2 T_{lmn}^{(2)} + \epsilon^3 T_{lmn}^{(3)} + \dots. \quad (3.9)$$

Note that the above expansion is straightforward since both S_{lmn} and T_{lmn} are linear in all the coefficients f_{lmn} . Thus the moment equations turn out to be

$$\begin{aligned} & \frac{\partial (f_{lmn}^{(0)} + \epsilon f_{lmn}^{(1)} + \epsilon^2 f_{lmn}^{(2)} + \epsilon^3 f_{lmn}^{(3)} + \dots)}{\partial t} \\ & + (S_{lmn}^{(0)} + \epsilon S_{lmn}^{(1)} + \epsilon^2 S_{lmn}^{(2)} + \epsilon^3 S_{lmn}^{(3)} + \dots) + (T_{lmn}^{(0)} + \epsilon T_{lmn}^{(1)} + \epsilon^2 T_{lmn}^{(2)} + \epsilon^3 T_{lmn}^{(3)} + \dots) \\ & = \frac{1}{\epsilon} \left(\frac{\rho \theta}{\mu} \sum_{n'=0}^{+\infty} a_{lmn'} \theta^{n-n'} \left(f_{lmn'}^{(0)} + \epsilon f_{lmn'}^{(1)} + \epsilon^2 f_{lmn'}^{(2)} + \epsilon^3 f_{lmn'}^{(3)} + \dots \right) \right). \end{aligned} \quad (3.10)$$

Matching the terms with the same orders with respect to ϵ , one obtains

$$\frac{\partial f_{lmn}^{(k)}}{\partial t} + S_{lmn}^{(k)} + T_{lmn}^{(k)} = \frac{\rho\theta}{\mu} \sum_{n'=0}^{+\infty} a_{lnn'} \theta^{n-n'} f_{lmn'}^{(k+1)}, \quad k \geq 0. \quad (3.11)$$

In Chapman-Enskog expansion, due to the assumption (3.8), the equation (3.11) is only applied to the case $(l, n) \neq (0, 0), (1, 0), (0, 1)$, in which the right-hand side of (3.11) is nonzero and (3.11) can provide us expressions for $f_{lmn}^{(k+1)}$. For more details about the Chapman-Enskog expansion, we refer the readers to textbooks such as [34]. In what follows, we are going to introduce a generalized version of the Chapman-Enskog expansion involving 13 moments in the assumption, which will be carried out below by studying each k incrementally. Note that the idea of the following method is also applicable for more general collision models.

3.2.1 First order ($k = 0$)

When $(l, n) \neq (0, 0), (1, 0), (0, 1)$, using (3.8) and the fact that S_{lmn} is a linear combination of (3.5), one can see that $f_{lmn}^{(0)} = S_{lmn}^{(0)} = 0$. Thus when $k = 0$, the equation (3.11) becomes

$$T_{lmn}^{(0)} = \frac{\rho\theta}{\mu} \sum_{n'=0}^{+\infty} a_{lnn'} \theta^{n-n'} f_{lmn'}^{(1)}. \quad (3.12)$$

If $l = 0, n > 1$ or $l \geq 3$, the property (P2) and (3.8) show that $T_{lmn}^{(0)} = 0$, meaning that

$$f_{lmn}^{(1)} = 0, \quad \text{if } l \geq 3 \text{ or } l = 0. \quad (3.13)$$

Below we focus on the cases $l = 1$ and $l = 2$. Note that $f_{1m0} = 0$, by which we can rewrite (3.12) as

$$T_{1mn}^{(0)} = \frac{\rho\theta}{\mu} \sum_{n'=1}^{+\infty} a_{1nn'} \theta^{n-n'} f_{1mn'}^{(1)}, \quad T_{2mn}^{(0)} = \frac{\rho\theta}{\mu} \sum_{n'=0}^{+\infty} a_{2nn'} \theta^{n-n'} f_{2mn'}^{(1)}. \quad (3.14)$$

Again by the property (P2) and (3.8), we see that $T_{1mn}^{(0)} = 0$ for all $n > 1$ and $T_{2mn}^{(0)} = 0$ for all $n > 0$. For any given m , the values of $f_{1mn'}^{(1)}$ and $f_{2mn'}^{(1)}$ can be solved from (3.14), and the result has the form:

$$f_{1mn}^{(1)} = \frac{\mu}{\rho\theta} A_{1n} \theta^{n-1} T_{1m1}^{(0)}, \quad f_{2mn}^{(1)} = \frac{\mu}{\rho\theta} A_{2n} \theta^n T_{2m0}^{(0)}, \quad (3.15)$$

where A_{1n} and A_{2n} are pure numbers. In principle, obtaining (3.15) requires solving an infinite matrix. In our implementation, this is approximated by a cutoff of the right-hand sides of (3.14) up to $n' \leq 9$.

Until now, our calculation is completely the same as the classical Chapman-Enskog expansion. In (3.15), all first order quantities can be represented by the conservative quantities and their derivatives (hidden in the expression of $T_{1m1}^{(0)}$ and $T_{2m0}^{(0)}$). However, to derive 13-moment equations, we are required to represent the distribution functions using more moments and less derivatives. For example, in Grad's 13-moment theory, no derivatives are included in the ansatz of the distribution function. In our derivation, this can be achieved by writing (3.15) as

$$f_{1mn}^{(1)} = \frac{A_{1n}}{A_{11}} \theta^{n-1} f_{1m1}^{(1)}, \quad f_{2mn}^{(1)} = \frac{A_{2n}}{A_{20}} \theta^n f_{2m0}^{(1)}. \quad (3.16)$$

Since f_{2m0} and f_{1m1} are included in the 13-moment theory, we mimic the assumption of Chapman-Enskog expansion (3.8) and set

$$f_{1m1} = \epsilon f_{1m1}^{(1)}, \quad f_{2m0} = \epsilon f_{2m0}^{(1)}, \quad f_{1m1}^{(k)} = f_{2m0}^{(k)} = 0, \quad k \geq 2. \quad (3.17)$$

By (3.16) and (3.17), we can write down the approximation of the distribution function up to first order in ϵ using the 13 moments:

$$\begin{aligned} f(\mathbf{x}, \boldsymbol{\xi}, t) \approx & \mathcal{M}(\mathbf{x}, \boldsymbol{\xi}, t) + \sum_{m=-1}^1 f_{1m1}(\mathbf{x}, t) \sum_{n=1}^{+\infty} \frac{A_{1n}}{A_{11}} [\theta(\mathbf{x}, t)]^{n-1} \psi_{1mn}(\mathbf{x}, \boldsymbol{\xi}, t) \\ & + \sum_{m=-2}^2 f_{2m0}(\mathbf{x}, t) \sum_{n=0}^{+\infty} \frac{A_{2n}}{A_{20}} [\theta(\mathbf{x}, t)]^n \psi_{2mn}(\mathbf{x}, \boldsymbol{\xi}, t), \end{aligned} \quad (3.18)$$

where we have written all the parameters t , \mathbf{x} and $\boldsymbol{\xi}$ for clarification. Note that in contrast to the Chapman-Enskog expansion of the distribution function, no derivatives are involved in the above expression. The equation (3.18) is also different from Grad's ansatz for the 13-moment theory, since (3.18) can be written equivalently as

$$\begin{aligned} f(\boldsymbol{\xi}) \approx & \left[1 - \sum_{i=1}^3 \frac{(\xi_i - v_i) q_i}{\theta^2} \sum_{n=1}^{+\infty} \frac{A_{1n}}{A_{11}} \sqrt{\frac{3\pi^{1/2} n!}{10\Gamma(n+5/2)}} L_n^{(3/2)} \left(\frac{\boldsymbol{\xi} - \mathbf{v}}{2\theta} \right) \right. \\ & \left. + \sum_{i=1}^3 \sum_{j=1}^3 \frac{\sigma_{ij} (\xi_i - v_i) (\xi_j - v_j)}{\theta^2} \sum_{n=0}^{+\infty} \frac{A_{2n}}{A_{20}} \sqrt{\frac{15\pi^{1/2} n!}{32\Gamma(n+7/2)}} L_n^{(5/2)} \left(\frac{\boldsymbol{\xi} - \mathbf{v}}{2\theta} \right) \right] \mathcal{M}(\boldsymbol{\xi}). \end{aligned} \quad (3.19)$$

Here $L_n^{(\alpha)}$ is the Laguerre polynomial defined in (B.2), and we have omitted the variables t and \mathbf{x} for conciseness. Grad's ansatz for the 13-moment theory can be obtained by truncating both infinite sums in (3.19) by preserving only their first terms, and therefore Grad's 13-moment theory does not fully represent the first-order term of the distribution function for general collision models. Due to the assumption (3.17), when we apply (3.11), equations for all the 13 moments should be excluded, i.e., $(l, n) \neq (0, 0), (0, 1), (1, 0), (1, 1), (2, 0)$.

Remark 3. The solvability of (3.14) relies on the existence of the spectral gap for the linearized Boltzmann collision operator. For IPL models, this has been proven in [29]. In particular, when $\eta = 5$, we have $A_{1n} = \delta_{1n}/a_{111}$ and $A_{2n} = \delta_{0n}/a_{200}$. In this case, the first two orders (3.18) are exactly the ansatz in Grad's 13-moment theory.

3.2.2 Second order ($k = 1$)

Now we set $k = 1$ in (3.11). Since $f_{000} = f_{001} = f_{1m0} = 0$ and $f_{2m0}^{(k)} = f_{1m1}^{(k)} = 0$ for $k \geq 2$, the result can be written as

$$\frac{\partial f_{lmn}^{(1)}}{\partial t} + S_{lmn}^{(1)} + T_{lmn}^{(1)} = \frac{\rho\theta}{\mu} \sum_{n'=n_0(l)}^{+\infty} a_{l n n'} \theta^{n-n'} f_{l m n'}^{(2)}, \quad (3.20)$$

where

$$n_0(l) = \begin{cases} 2, & \text{if } l = 0, 1, \\ 1, & \text{if } l = 2, \\ 0, & \text{if } l \geq 3. \end{cases} \quad (3.21)$$

Since $f_{lmn}^{(1)}$ has been fully obtained in the previous section (see (3.13) and (3.17)), the expressions of $S_{lmn}^{(1)}$ and $T_{lmn}^{(1)}$ can be naturally obtained. Thus the left-hand side of (3.20) can already be represented by the 13 moments. To obtain the second-order contributions $f_{lmn}^{(2)}$, for any l and m , we just need to solve the infinite linear system (3.20), and the general result is

$$f_{lmn}^{(2)} = \frac{\mu}{\rho\theta} \sum_{n'=n_0(l)}^{+\infty} B_{lmn'} \theta^{n-n'} \left(\frac{\partial f_{lmn'}^{(1)}}{\partial t} + S_{lmn'}^{(1)} + T_{lmn'}^{(1)} \right), \quad (3.22)$$

where $B_{lmn'}$ are all pure numbers. In our implementation, we again truncate the system (3.20) at $n' = \lfloor 10 - l/2 \rfloor$. For the purpose of deriving R13 equations, we only need $f_{lmn}^{(2)}$ up to $l = 4$.

The right-hand side of (3.22) still contains time derivatives, which are not desired. In general, they can all be replaced by spatial derivatives. Note that $\partial_t f_{lmn}^{(1)}$ is nonzero only if $l = 1$ or $l = 2$. In these cases, we have

$$\begin{aligned} \frac{\partial f_{1mn'}^{(1)}}{\partial t} &= \frac{A_{1n'}}{A_{11}} \left(\theta^{n'-1} \frac{\partial f_{1m1}^{(1)}}{\partial t} + (n'-1) \theta^{n'-2} \frac{\partial \theta}{\partial t} f_{1m1}^{(1)} \right), \\ \frac{\partial f_{2mn'}^{(1)}}{\partial t} &= \frac{A_{2n'}}{A_{20}} \left(\theta^{n'} \frac{\partial f_{2m0}^{(1)}}{\partial t} + n' \theta^{n'-1} \frac{\partial \theta}{\partial t} f_{2m0}^{(1)} \right). \end{aligned} \quad (3.23)$$

We first focus on $\partial_t f_{1m1}^{(1)}$ and $\partial_t f_{2m0}^{(1)}$. Taking $\partial_t f_{1m1}^{(1)}$ as an example, we do the following calculation:

$$\begin{aligned} & \frac{\partial f_{1m1}^{(1)}}{\partial t} + \frac{1}{\epsilon} \left(S_{1m1}^{(0)} + T_{1m1}^{(0)} \right) + \left(S_{1m1}^{(1)} + T_{1m1}^{(1)} \right) \\ &= \frac{1}{\epsilon} \frac{\rho\theta}{\mu} \sum_{n=1}^{+\infty} a_{11n} \theta^{1-n} f_{1mn}^{(1)} + \frac{\rho\theta}{\mu} \sum_{n=1}^{+\infty} a_{11n} \theta^{1-n} f_{1mn}^{(2)} + \mathcal{O}(\epsilon) \\ &= \frac{1}{\epsilon} \frac{\rho\theta}{\mu} \frac{f_{1m1}^{(1)}}{A_{11}} + \sum_{n=2}^{+\infty} a_{11n} \theta^{1-n} \sum_{n'=2}^{+\infty} B_{1nn'} \theta^{n-n'} \left(\frac{\partial f_{lmn'}^{(1)}}{\partial t} + S_{lmn'}^{(1)} + T_{lmn'}^{(1)} \right) + \mathcal{O}(\epsilon) \\ &= \frac{1}{\epsilon} \frac{\rho\theta}{\mu} \frac{f_{1m1}^{(1)}}{A_{11}} + \frac{1}{A_{11}} \sum_{n=2}^{+\infty} \sum_{n'=2}^{+\infty} a_{11n} B_{1nn'} A_{1n'} \left(\frac{\partial f_{1m1}^{(1)}}{\partial t} + \frac{n'-1}{\theta} \frac{\partial \theta}{\partial t} f_{1m1}^{(1)} \right) \\ & \quad + \sum_{n'=2}^{+\infty} \left(\sum_{n=2}^{+\infty} a_{11n} B_{1nn'} \right) \theta^{1-n'} \left(S_{lmn'}^{(1)} + T_{lmn'}^{(1)} \right) + \mathcal{O}(\epsilon), \end{aligned} \quad (3.24)$$

from which it can be solved that

$$\begin{aligned} \frac{\partial f_{1m1}^{(1)}}{\partial t} &= \left(1 - \sum_{n'=2}^{+\infty} \lambda_{1n'} \right)^{-1} \left[\frac{1}{\epsilon} \left(\frac{\rho\theta}{\mu} \frac{f_{1m1}^{(1)}}{A_{11}} - T_{1m1}^{(0)} \right) \right. \\ & \quad \left. + \sum_{n'=2}^{+\infty} \frac{(n'-1)\lambda_{1n'}}{\theta} \frac{\partial \theta}{\partial t} f_{1m1}^{(1)} + \sum_{n'=1}^{+\infty} C_{1n'} \theta^{1-n'} \left(S_{1mn'}^{(1)} + T_{1mn'}^{(1)} \right) \right] + \mathcal{O}(\epsilon), \end{aligned} \quad (3.25)$$

where we have used $S_{1m1}^{(0)} = 0$, and the newly introduced constants are

$$C_{ln'} = \begin{cases} -1, & \text{if } n' = n_0(l) - 1, \\ \sum_{n=n_0(l)}^{+\infty} a_{l,n_0(l)-1,n} B_{lnn'}, & \text{if } n' \geq n_0(l), \end{cases} \quad \lambda_{ln'} = \frac{C_{ln'} A_{ln'}}{A_{l,n_0(l)-1}}. \quad (3.26)$$

Similarly, we can obtain

$$\begin{aligned} \frac{\partial f_{2m0}^{(1)}}{\partial t} = & \left(1 - \sum_{n'=1}^{+\infty} \lambda_{2n'}\right)^{-1} \left[\frac{1}{\epsilon} \left(\frac{\rho\theta}{\mu} \frac{f_{2m0}^{(1)}}{A_{20}} - T_{2m0}^{(0)} \right) \right. \\ & \left. + \sum_{n'=1}^{+\infty} \frac{n'\lambda_{2n'}}{\theta} \frac{\partial\theta}{\partial t} f_{2m0}^{(1)} + \sum_{n'=0}^{+\infty} C_{2n'} \theta^{-n'} \left(S_{2mn'}^{(1)} + T_{2mn'}^{(1)} \right) \right] + \mathcal{O}(\epsilon), \end{aligned} \quad (3.27)$$

As a summary, the time derivatives in (3.22) can be replaced with spatial derivatives by the following operations:

- If $l \neq 1$ and $l \neq 2$, set the derivative $\partial_t f_{lmn'}^{(1)}$ to be zero. If $l = 1$ or $l = 2$, replace $\partial_t f_{1mn'}^{(1)}$ by (3.23)(3.25)(3.27).
- After replacement, the results still include the time derivatives of \mathbf{v} and θ . These terms can be replaced by conservation laws (2.2). In fact, we can use the fact that σ_{kl} and q_k are $\mathcal{O}(\epsilon)$ terms to rewrite the conservation laws of momentum and energy as

$$\frac{\partial v_i}{\partial t} = -v_k \frac{\partial v_i}{\partial x_k} - \frac{\theta}{\rho} \frac{\partial \rho}{\partial x_i} - \frac{\partial \theta}{\partial x_i} + \mathcal{O}(\epsilon), \quad \frac{\partial \theta}{\partial t} = -\frac{2}{3} \theta \frac{\partial v_k}{\partial x_k} - v_k \frac{\partial \theta}{\partial x_k} + \mathcal{O}(\epsilon), \quad (3.28)$$

and use these equations for substitution.

- After the above replacements, the $\mathcal{O}(\epsilon)$ terms can be dropped.

By now, we have presented all the coefficients $f_{lmn}^{(2)}$ by the 13 moments and their spatial derivatives. When $l = 1, 2$, the results include a coefficient $1/\epsilon$ coming from (3.25) and (3.27). More precisely, $f_{1mn}^{(2)}$ and $f_{2mn}^{(2)}$ have the form

$$f_{1mn}^{(2)} = \frac{1}{\epsilon} \theta^{n-1} \left(\sum_{n'=2}^{+\infty} B_{1nn'} \frac{A_{1n'}}{A_{11}} \right) \left(1 - \sum_{n'=2}^{+\infty} \lambda_{1n'} \right)^{-1} \left(\frac{f_{1m1}^{(1)}}{A_{11}} - \frac{\mu}{\rho\theta} T_{1m1}^{(0)} \right) + W_{1mn}^{(2)}, \quad n \geq 2, \quad (3.29)$$

$$f_{2mn}^{(2)} = \frac{1}{\epsilon} \theta^n \left(\sum_{n'=1}^{+\infty} B_{2nn'} \frac{A_{2n'}}{A_{20}} \right) \left(1 - \sum_{n'=1}^{+\infty} \lambda_{2n'} \right)^{-1} \left(\frac{f_{2m0}^{(1)}}{A_{20}} - \frac{\mu}{\rho\theta} T_{2m0}^{(0)} \right) + W_{2mn}^{(2)}, \quad n \geq 1, \quad (3.30)$$

where $W_{1mn}^{(2)}$ and $W_{2mn}^{(2)}$ are terms independent of ϵ . Note that only first-order derivatives have been introduced into $f_{lmn}^{(2)}$, while in the original Chapman-Enskog expansion, the second-order (Burnett-order) term $f^{(2)}$ includes second-order derivatives.

3.2.3 Third order ($k = 2$)

Similar to the case $k = 1$, when $k = 2$, we can solve the linear system (3.11) to get

$$f_{lmn}^{(3)} = \frac{\mu}{\rho\theta} \sum_{n'=n_0(l)}^{+\infty} B_{lmn'} \theta^{n-n'} \left(\frac{\partial f_{lmn'}^{(2)}}{\partial t} + S_{lmn'}^{(2)} + T_{lmn'}^{(2)} \right), \quad n \geq n_0(l). \quad (3.31)$$

After inserting the expression of $f_{lmn}^{(2)}$ into the above equation, we again need to deal with the time derivatives. The time derivatives appearing in $S_{lmn'}^{(2)}$ can again be replaced by (3.28) without $\mathcal{O}(\epsilon)$ terms. Below we focus only the time derivative of $f_{lmn'}^{(2)}$.

When $l \neq 1$ and $l \neq 2$, the second-order term $f_{lmn}^{(2)}$ does not include the coefficient $1/\epsilon$, and therefore $\partial_t f_{lmn}^{(2)}$ can be computed by inserting the expression of $f_{lmn}^{(2)}$, expanding the time derivative, and then replacing the time derivative of each moment in (3.3) by (3.28)(3.25)(3.27) and the continuity equation $\partial_t \rho = -\text{div}(\rho \mathbf{v})$. After replacement, we can also safely drop the $\mathcal{O}(\epsilon)$ terms. The treatment for $l = 1, 2$ is more complicated, and the process will be detailed below.

When $l = 1$ and $n \geq 2$ (the case $l = 2, n \geq 1$ is similar), by (3.29),

$$\begin{aligned} \frac{\partial f_{1mn}^{(2)}}{\partial t} &= \frac{1}{\epsilon} \theta^{n'-1} \frac{D_{1n'}}{A_{11}} \frac{\partial f_{1m1}^{(1)}}{\partial t} - \frac{1}{\epsilon} \theta^{n'-1} D_{1n'} \frac{\partial}{\partial t} \left(\frac{\mu}{\rho \theta} T_{1m1}^{(0)} \right) \\ &+ \frac{1}{\epsilon} (n' - 1) \theta^{n'-2} D_{1n'} \left(\frac{f_{1m1}^{(1)}}{A_{11}} - \frac{\mu}{\rho \theta} T_{1m1}^{(0)} \right) \frac{\partial \theta}{\partial t} + \frac{\partial W_{1mn}^{(2)}}{\partial t}, \end{aligned} \quad (3.32)$$

where

$$D_{1n} = \left(\sum_{n'=2}^{+\infty} B_{1nn'} \frac{A_{1n'}}{A_{11}} \right) \left(1 - \sum_{n'=2}^{+\infty} \lambda_{1n'} \right)^{-1}. \quad (3.33)$$

The last term $\partial_t W_{1mn}^{(2)}$ is independent of ϵ , and therefore the time derivative can also be replaced by conservation laws and (3.25)(3.27) without $\mathcal{O}(\epsilon)$ terms. However, for the first three terms on the right-hand side of (3.32), due to the existence of $1/\epsilon$, when replaced by spatial derivatives, the $\mathcal{O}(\epsilon)$ terms have to be taken into account to capture the $\mathcal{O}(1)$ contribution. Note that $T_{1m1}^{(0)}$ also appears in (3.15), where the first equation for $n = 1$ represents Fourier's law. We know that $(\rho \theta)^{-1} T_{1m1}^{(0)}$ is essentially the spatial derivative of θ multiplied by a constant. Therefore the second and third terms involve only the time derivative of density ρ and temperature θ , and they can be replaced exactly by the conservation laws (2.2). Thus the only troublesome term is again $\partial_t f_{1m1}^{(1)}$. Before discussing this term, we first implement all the aforementioned replacements and write the result as

$$f_{1mn}^{(3)} = \frac{1}{\epsilon} \frac{\mu}{\rho \theta} \frac{\theta^{n-1}}{A_{11}} \left(\sum_{n'=2}^{+\infty} B_{1nn'} D_{1n'} \right) \frac{\partial f_{1m1}^{(1)}}{\partial t} + R_{1mn}^{(3)},$$

where $R_{1mn}^{(3)}$ is the collection of terms which does not include any time derivatives.

By now, we can carry out the calculation similar to (3.24):

$$\begin{aligned} &\frac{\partial f_{1m1}^{(1)}}{\partial t} + \frac{1}{\epsilon} \left(S_{1m1}^{(0)} + T_{1m1}^{(0)} \right) + \left(S_{1m1}^{(1)} + T_{1m1}^{(1)} \right) + \epsilon \left(S_{1m1}^{(2)} + T_{1m1}^{(2)} \right) \\ &= \frac{1}{\epsilon} \frac{\rho \theta}{\mu} \sum_{n=1}^{+\infty} a_{11n} \theta^{1-n} f_{1mn}^{(1)} + \frac{\rho \theta}{\mu} \sum_{n=1}^{+\infty} a_{11n} \theta^{1-n} f_{1mn}^{(2)} + \epsilon \frac{\rho \theta}{\mu} \sum_{n=1}^{+\infty} a_{11n} \theta^{1-n} f_{1mn}^{(3)} + \mathcal{O}(\epsilon^2) \\ &= \frac{1}{\epsilon} \frac{\rho \theta}{\mu} \frac{f_{1m1}^{(1)}}{A_{11}} + \frac{\rho \theta}{\mu} \sum_{n=2}^{+\infty} a_{11n} \theta^{1-n} f_{1mn}^{(2)} \\ &\quad + \sum_{n=2}^{+\infty} \frac{a_{11n}}{A_{11}} \sum_{n'=2}^{+\infty} B_{1nn'} D_{1n'} \frac{\partial f_{1m1}^{(1)}}{\partial t} + \epsilon \frac{\rho \theta}{\mu} \sum_{n=2}^{+\infty} a_{11n} \theta^{1-n} R_{1mn}^{(3)} + \mathcal{O}(\epsilon^2), \end{aligned} \quad (3.34)$$

Solving $\partial_t f_{1m1}^{(1)}$ from the above equation, we get

$$\begin{aligned} \frac{\partial f_{1m1}^{(1)}}{\partial t} = & \left(1 - \frac{1}{A_{11}} \sum_{n'=2}^{+\infty} C_{1n'} D_{1n'} \right)^{-1} \left[\frac{1}{\epsilon} \left(\frac{\rho\theta}{\mu} \frac{f_{1m1}^{(1)}}{A_{11}} - T_{1m1}^{(0)} \right) \right. \\ & + \left(\frac{\rho\theta}{\mu} \sum_{n=2}^{+\infty} a_{11n} \theta^{1-n} f_{1mn}^{(2)} - \left(S_{1m1}^{(1)} + T_{1m1}^{(1)} \right) \right) \\ & \left. + \epsilon \left(\frac{\rho\theta}{\mu} \sum_{n=2}^{+\infty} a_{11n} \theta^{1-n} R_{1mn}^{(3)} - \left(S_{1m1}^{(2)} + T_{1m1}^{(2)} \right) \right) \right] + \mathcal{O}(\epsilon^2). \end{aligned} \quad (3.35)$$

In (3.35), the time derivatives in $S_{1m1}^{(2)}$ can be replaced by (3.28) with $\mathcal{O}(\epsilon)$ terms dropped, while the time derivatives in $S_{1m1}^{(1)}$ had to be replaced by complete conservation laws (2.2). The last step is to substitute the above equation into (3.2.3), and the $\mathcal{O}(\epsilon^2)$ term in (3.35) can now be discarded. This completes the calculation of $f_{1mn}^{(3)}$.

The calculation of $f_{2mn}^{(3)}$ follows exactly the same procedure, and the details are omitted. The above procedure shows that the expression of $f_{lmn}^{(3)}$ includes second-order derivatives of the 13 moments.

3.3 Thirteen moment equations

With all the moments up to third order calculated, we are ready to write down the 13-moment equations. Note that all the 13-moment equations include the conservation laws (2.2). Therefore we focus only on the equations for σ_{ij} and q_j , or equivalently, f_{2m0} and f_{1m1} . Since $f_{2m0} = \epsilon f_{2m0}^{(1)}$ and $f_{1m1} = \epsilon f_{1m1}^{(1)}$, these equations are to be obtained by truncation of (3.10). Two different truncations are considered below, which correspond to GG13 equations and R13 equations, respectively.

3.3.1 Generalized Grad's 13-moment equations

The derivation of GG13 equations is basically a truncation of (3.10) up to the first order. The result reads

$$\begin{aligned} \epsilon \frac{\partial f_{2m0}^{(1)}}{\partial t} + \epsilon S_{2m0}^{(1)} + T_{2m0}^{(0)} + \epsilon T_{2m0}^{(1)} &= \frac{\rho\theta}{\mu} \left(\frac{1}{A_{20}} f_{2m0}^{(1)} + \epsilon \sum_{n'=1}^{+\infty} a_{20n'} \theta^{-n'} f_{2mn'}^{(2)} \right), \\ \epsilon \frac{\partial f_{1m1}^{(1)}}{\partial t} + \epsilon S_{1m1}^{(1)} + T_{1m1}^{(0)} + \epsilon T_{1m1}^{(1)} &= \frac{\rho\theta}{\mu} \left(\frac{1}{A_{11}} f_{1m1}^{(1)} + \epsilon \sum_{n'=2}^{+\infty} a_{11n'} \theta^{1-n'} f_{1mn'}^{(2)} \right), \end{aligned} \quad (3.36)$$

where we have used

$$\sum_{n'=0}^{+\infty} a_{20n'} \theta^{-n'} f_{2mn'}^{(1)} = \sum_{n'=0}^{+\infty} a_{20n'} \frac{A_{2n'}}{A_{20}} f_{2m0}^{(1)} = \frac{1}{A_{20}} f_{2m0}^{(1)}, \quad (3.37)$$

$$\sum_{n'=1}^{+\infty} a_{11n'} \theta^{1-n'} f_{1mn'}^{(1)} = \sum_{n'=1}^{+\infty} a_{11n'} \frac{A_{1n'}}{A_{11}} f_{1m1}^{(1)} = \frac{1}{A_{11}} f_{1m1}^{(1)}. \quad (3.38)$$

All the terms in (3.36) have been represented by the 13 moments (3.3) and their derivatives in Section 3.2, and the time derivatives in $S_{2m0}^{(1)}$ can be replaced by (3.28) with $\mathcal{O}(\epsilon)$ terms

discarded. The final step is to revert the scaling of space and time introduced in the beginning of Section 3.2, which can be simply achieved by setting ϵ to be 1.

This set of equations are called generalized Grad's 13-moment (GG13) equations as proposed in [37]. Similar to Grad's 13-moment equations, the GG13 equations are also first-order quasi-linear equations. However, they are different from Grad's 13-moment equations in two ways: (1) in Grad's 13-moment equations, the terms $T_{1m1}^{(1)}$ and $T_{2m0}^{(1)}$ come directly from the truncation of the distribution function, while in generalized Grad's 13-moment equations, they include information from inversion of the linearized collision operator; (2) in Grad's 13-moment equations, the collision term does not include information from $f_{1mn'}$ with $n' > 1$ or $f_{2mn'}$ with $n' > 0$. Due to such differences, as mentioned in Section 2.3, Grad's 13-moment equations are accurate only up to first order for general IPL models.

Now we compare the equations (3.36) with the equations (2.3). On the left-hand side, we can see from (3.36) that no second-order terms are involved. Since the moments m_{ijk} (f_{3m0}), R_{ik} (f_{2m1}) and Δ (f_{002}) are all $O(\epsilon^2)$ terms, they are simply set to be zero in GG13 equations. The right-hand side is much more complicated due to the involved formulas for second-order terms. We would just like to point out that the coefficient $D_0^{(\eta)}$ in (2.4) does not equal the coefficient $1/A_{20}$ in (3.36), since the same term also appears in $f_{2mn}^{(2)}$, as is shown in (3.30). Due to the similar reason, the coefficient $E_0^{(\eta)}$ in (2.4) does not equal $1/A_{11}$ in (3.36).

3.3.2 Regularized 13-moment equations

To gain one more order of accuracy, we need to keep the second-order terms in (3.10), and the result is

$$\begin{aligned} \epsilon \frac{\partial f_{2m0}^{(1)}}{\partial t} + \epsilon S_{2m0}^{(1)} + \epsilon^2 S_{2m0}^{(2)} + T_{2m0}^{(0)} + \epsilon T_{2m0}^{(1)} + \epsilon^2 T_{2m0}^{(2)} = \\ \frac{\rho\theta}{\mu} \left(\frac{1}{A_{20}} f_{2m0}^{(1)} + \sum_{n'=1} a_{2nn'} \theta^{n-n'} \left(\epsilon f_{2mn'}^{(2)} + \epsilon^2 f_{2mn'}^{(3)} \right) \right), \\ \epsilon \frac{\partial f_{1m1}^{(1)}}{\partial t} + \epsilon S_{1m1}^{(1)} + \epsilon^2 S_{1m1}^{(2)} + T_{1m1}^{(0)} + \epsilon T_{1m1}^{(1)} + \epsilon^2 T_{1m1}^{(2)} = \\ \frac{\rho\theta}{\mu} \left(\frac{1}{A_{11}} f_{1m1}^{(1)} + \sum_{n'=2} a_{1nn'} \theta^{n-n'} \left(\epsilon f_{1mn'}^{(2)} + \epsilon^2 f_{1mn'}^{(3)} \right) \right). \end{aligned} \quad (3.39)$$

Again, the time derivatives for velocity and temperature in $S_{2m0}^{(i)}$ and $S_{1m1}^{(i)}$, $i = 1, 2$ need to be replaced by spatial derivatives. In order to preserve the second-order terms, the time derivatives in $S_{2m0}^{(1)}$ and $S_{1m1}^{(1)}$ need to be substituted by the complete conservation laws (2.2), where as in $S_{2m0}^{(2)}$ and $S_{1m1}^{(2)}$, the replacement of time derivatives are done by using (3.28) and discarding $\mathcal{O}(\epsilon)$ terms. Afterwards, we set ϵ to be 1, and the result is regularized 13-moment equations.

By replacing all the coefficients with the primitive variables σ_{ij} and q_i , the equations (2.3) with (2.4)(2.6) and (C.1)(C.2) can be obtained. Compared with the linear R13 equations obtained in [37], much more information is included in this nonlinear version. For instance, in (2.6), one can see that all the first three terms in $m_{ijk}^{(\eta)}$ are nonlinear and all the last three terms in $\Delta^{(\eta)}$ are nonlinear. Clearly these terms cannot be ignored in problem such as the structure of plane shock waves, which will be studied in the following section.

4 Numerical examples

In this section, we are going to test the behavior of the nonlinear R13 equations by computing the structure of one-dimensional plane shock waves, which is a benchmark problem in the gas kinetic theory. It involves strong nonequilibrium, but does not have any boundary condition, which makes it suitable for testing the ability of describing nonequilibrium processes for our models.

For one-dimensional flow, the moments satisfy

$$v_2 = v_3 = 0, \quad \sigma_{12} = \sigma_{13} = \sigma_{23} = 0, \quad \sigma_{22} = \sigma_{33} = -\frac{1}{2}\sigma_{11}, \quad q_2 = q_3 = 0. \quad (4.1)$$

For simplicity, we use the notation $v = v_1$, $\sigma = \sigma_{11}$ and $q = q_1$. Then thirteen moments are reduced to five moments ρ , v , θ , σ and q . Below we write down the R13 model for these quantities in the form of balance laws:

$$\begin{aligned} \rho_t + (\rho v)_x &= 0, \\ (\rho v)_t + (\rho v^2 + \rho\theta + \sigma)_x &= 0, \\ \left(\frac{1}{2}\rho v^2 + \frac{3}{2}\rho\theta\right)_t + \left(q + \frac{1}{2}\rho v^3 + \frac{5}{2}\rho v\theta + v\sigma\right)_x &= 0, \\ (\rho v^2 + \rho\theta + \sigma)_t + \left(\frac{6}{5}q + \rho v^3 + 3\rho v\theta + 3v\sigma + m^{(\eta)}\right)_x &= \Sigma_{1D}^{(\eta)}, \\ \left(q + \frac{1}{2}\rho v^3 + \frac{5}{2}\rho v\theta + v\sigma\right)_t + (\text{FQ})_x &= Q_{1D}^{(\eta)} + v\Sigma_{1D}^{(\eta)}, \end{aligned} \quad (4.2)$$

where

$$\text{FQ} = \frac{16}{5}vq + \frac{1}{2}\rho v^4 + 4v^2\theta + \frac{5}{2}\rho\theta^2 + \frac{5}{2}v^2\sigma + \left(\frac{7}{2} - \sqrt{\frac{14}{3}}C_{1D}^{(\eta)}\right)\theta\sigma + m^{(\eta)}v + \frac{1}{2}R^{(\eta)} + \frac{1}{6}\Delta^{(\eta)}, \quad (4.3)$$

with $m^{(\eta)}$, $R^{(\eta)}$, $\Delta^{(\eta)}$ being $m_{111}^{(\eta)}$, $R_{11}^{(\eta)}$ and $\Delta^{(\eta)}$ in (2.6) substituted by (4.1). On the right-hand side, $\Sigma_{1D}^{(\eta)}$ and $Q_{1D}^{(\eta)}$ are, respectively, $\Sigma_{11}^{(\eta,1)} + \Sigma_{11}^{(\eta,2)}$ and $Q_1^{(\eta,1)} + Q_1^{(\eta,2)}$ in (2.3) subject to (4.1). The constant $C_{1D}^{(\eta)}$ depends only on η , and some of its values are listed in Table 5.

η	5	7	10	17	∞
$C_{1D}^{(\eta)}$	0	0.0331	0.0553	0.0748	0.1

Table 5: Coefficient $C_{1D}^{(\eta)}$ for different η .

The structure of plane shock waves with Mach number Ma can be obtained by setting the initial data to be

$$(\rho, v, \theta, \sigma, q) = \begin{cases} (\rho_l, v_l, \theta_l, 0, 0), & x < 0, \\ (\rho_r, v_r, \theta_r, 0, 0), & x > 0, \end{cases} \quad (4.4)$$

where

$$\begin{aligned} \rho_l &= 1, & v_l &= \sqrt{5/3}Ma, & \theta_l &= 1, \\ \rho_r &= \frac{4Ma^2}{Ma^2 + 3}, & v_r &= \sqrt{\frac{5}{3} \frac{Ma^2 + 3}{4Ma}}, & \theta_r &= \frac{5Ma^2 - 1}{4\rho_r}. \end{aligned}$$

To solve (4.2) and (4.4) numerically, the finite volume method is adopted. Since the left-hand side of (4.2) has the form of a conservation law, we apply the HLL scheme in the discretization. The right-hand side provides the non-conservative part, for which central difference method is used to approximate both the first and second derivatives. For the time discretization, we use the classical forward Euler method in all the examples. The DSMC results for variable hard sphere models with the same viscosity index are used as reference solutions [3].

4.1 Shock structure for Maxwell molecules

This section is devoted to shock structure computation of Maxwell molecules. The same computation has been carried out in [40], and the main purpose of this section is the verification of our numerical method and the comparison between linearized and quadratic collision terms. Note that the R13 equations for Maxwell molecules with quadratic collision terms are already available to us [35]. Two Mach numbers 1.55 and 9.0 are tested, and we show the numerical results for all the moments in Figures 5 and 6, where the density, velocity and temperature are given in their normalized form:

$$\bar{\rho} = \frac{\rho - \rho_l}{|\rho_r - \rho_l|}, \quad \bar{v} = \frac{v - v_r}{|v_l - v_r|}, \quad \bar{\theta} = \frac{\theta - \theta_l}{|\theta_r - \theta_l|}.$$

For the small Mach number 1.55, both linearized and quadratic collision terms provide good agreement with DSMC results, except for a slight underestimation of the peak heat flux. Surprisingly, when the Mach number reaches 9.0, R13 equations with linearized and quadratic collision terms still provide almost identical shock structure. Similar to the results in [40], our profiles also show some typical structures for R13 solutions with high Mach numbers, such as kinks in the profiles and a too fast decay in the low-density region, which indicates the correctness of our simulation. As is stated in [40], the underpredicted heat flux is due to the loss of some fourth-order terms in the regularized moment equations. Nevertheless, these results indicate that quadratic collision terms do not contribute too much to the shock structure for Mach number lower than 9.0.

4.2 Shock structures for different Mach numbers

In this experiment, we test the approximability of the R13 model by varying the Mach number for a non-Maxwell collision model. Four Mach numbers $Ma = 1.55, 3.0, 6.5, 9.0$ are taken into account, and we consider the inverse power law model with $\eta = 10$ and the hard-sphere model ($\eta = \infty$) in our tests.

Figure 7 and 8 show the comparison between the R13 results and the DSMC results for $\eta = 10$. The profiles of all the five quantities have been plotted. Although DSMC uses variable hard sphere model as an approximation of the inverse power law model, the simulation results in [22] show that for the shock structure problem, the variable hard sphere model and the inverse power law model show almost identical results for Mach numbers 6.5 and 9.0, which means that it is reliable to use DSMC results to check the quality of R13 results. For increasing Mach number, it is generally harder for macroscopic models to accurately capture the nonequilibrium effects. This can be clearly observed from Figure 8, which shows that the heat flux is underestimated in the low density region. Note that the shock structure in the high density region is well captured for all Knudsen numbers, since the high density and temperature in this region result in distribution functions close to the local Maxwellians, which can be relatively easier to represent using the Chapman-Enskog expansion.

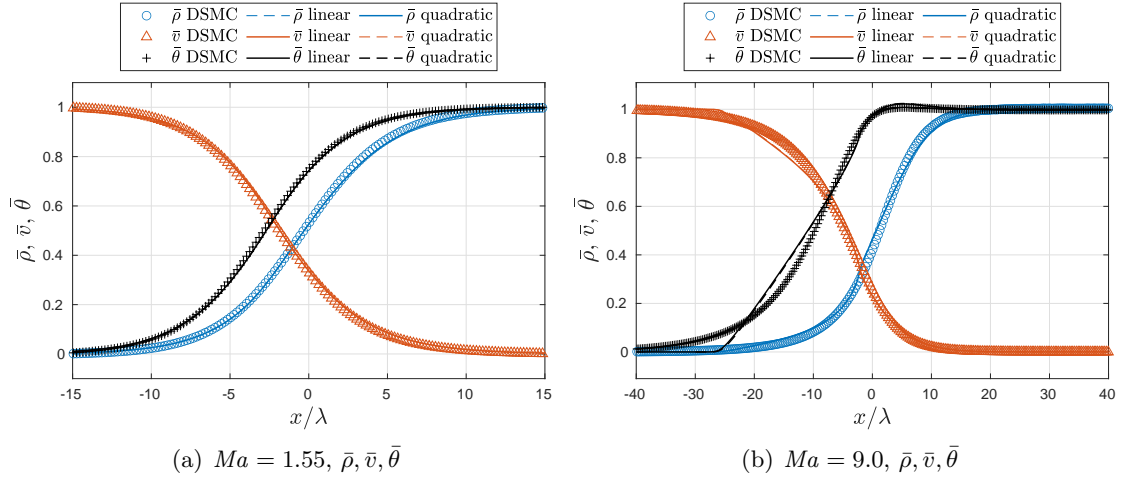


Figure 5: Normalized density, velocity, and temperature of shock structures for the Maxwell molecules model and Mach numbers $Ma = 1.55, 9$. DSMC solutions for the variable hard sphere model are provided as reference results. The horizontal axis is x/λ with λ being the mean free path. The solid lines are the numerical results for the linearized collision model and the dashed lines are those for the quadratic collision model.

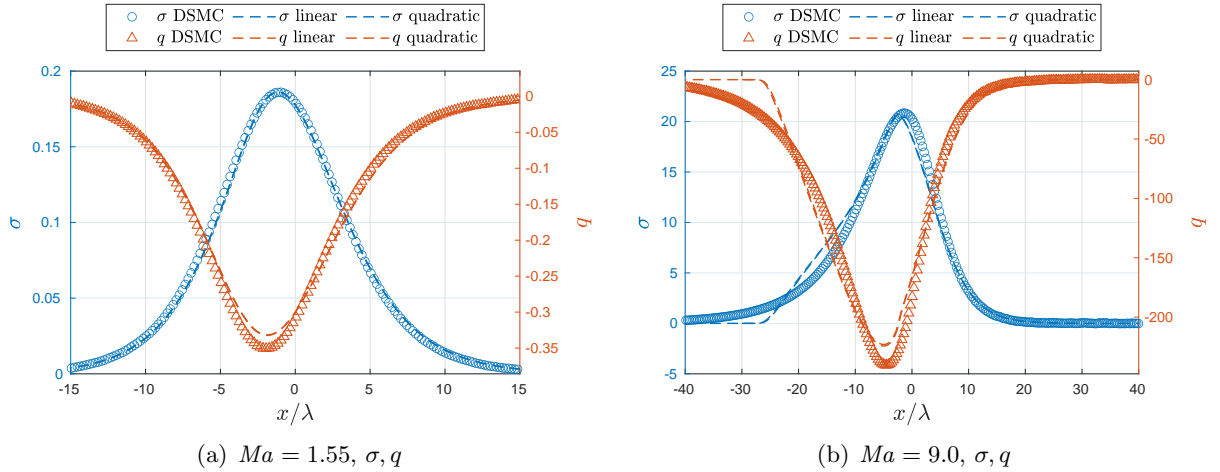


Figure 6: The stress σ and heat flux q of shock structures for the Maxwell molecules model and Mach numbers $Ma = 1.55, 9$. DSMC results for the variable hard sphere model are provided as references. The horizontal axis is x/λ with λ being the mean free path. The left y -axis corresponds to the stress and the right y -axis corresponds to the heat flux. The solid lines are the numerical results for the linearized collision model and the dashed lines are those for the quadratic collision model.

Figure 9 and 10 show the shock structures for the same Mach numbers for the hard sphere model. Similarly, the normalized density $\bar{\rho}$, velocity \bar{v} , and temperature $\bar{\theta}$ are plotted in Figure 9. It is interesting that when the Mach number increases from 3.0 to 9.0, there is no significant decrement of the general quality of R13 approximation. In [44], the authors calculated shock structure for the hard-sphere model using the R13 equations for Maxwell molecules with its expression of viscosity changed to match the hard-sphere model. At Mach number 3.0, such a method already shows significant deviation in the profile of heat flux. After switching to the

“true” R13 equations for hard spheres, much better agreement can be obtained. Note that the peak of the heat flux is again underestimated in all results (including the model with $\eta = 10$). In general, up to Mach number 9.0, R13 results show quite satisfactory agreement with the reference solutions for both models.

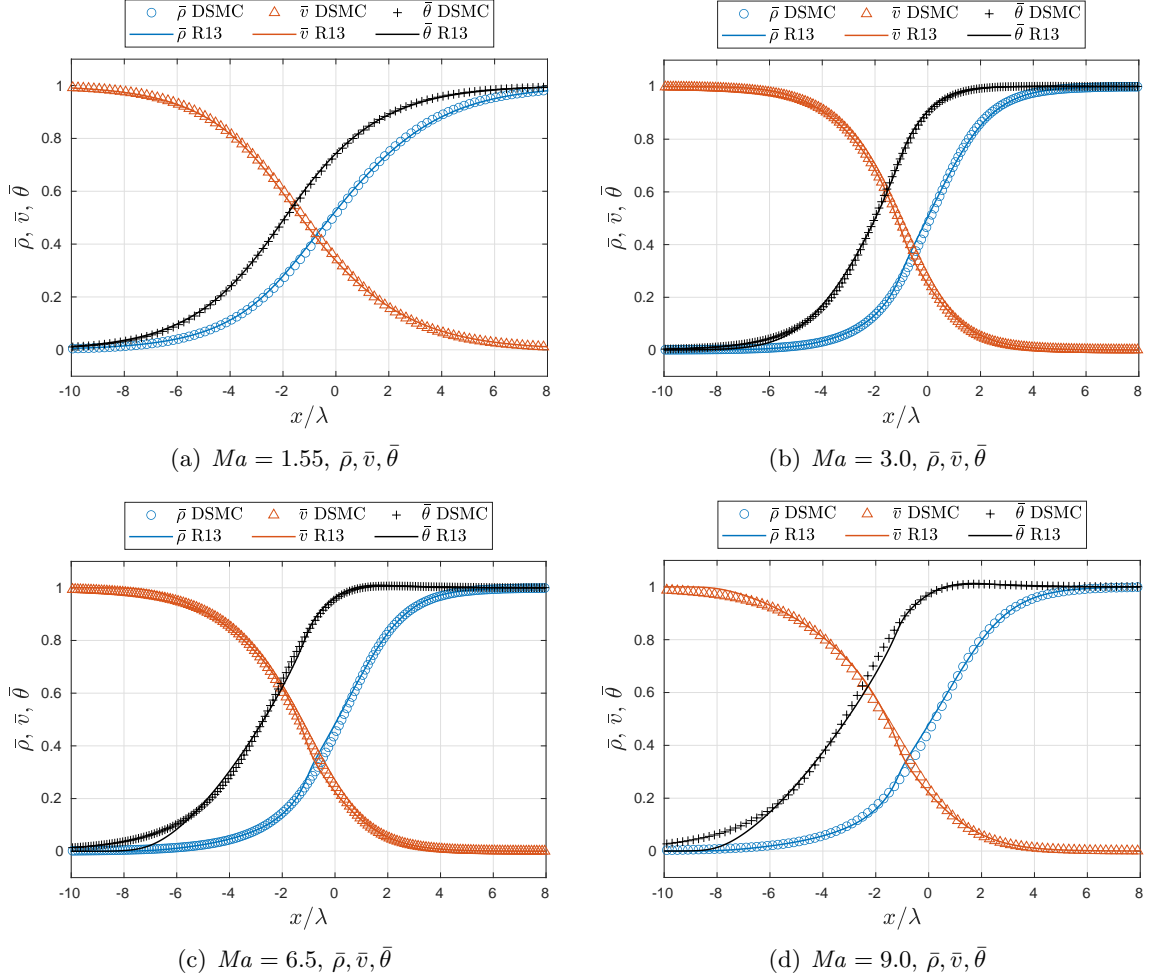


Figure 7: Normalized density, velocity, and temperature of shock structures for the IPL model with $\eta = 10$ and Mach numbers $Ma = 1.55, 3, 6.5, 9$. DSMC solutions for the variable hard sphere model are provided as reference results. The horizontal axis is x/λ with λ being the mean free path.

4.3 Shock structures for different indices η

Now we perform the tests by fixing the Mach number as $Ma = 6.5$ and changing the parameter η . Here we focus only on hard potentials with $\eta = 7, 10, 17$ and ∞ (hard-sphere model). The results for all the five quantities are plotted in Figure 11 and 12. Similarly, the normalized density $\bar{\rho}$, velocity \bar{v} , and temperature $\bar{\theta}$ are plotted in Figure 11. Both R13 results and DSMC results show that the shock structure differs for different collision models, and it can be observed that better agreement between two results can be achieved for larger η . The possible reason is that larger η gives smaller viscosity index, which brings the distribution function closer to the local Maxwellian.

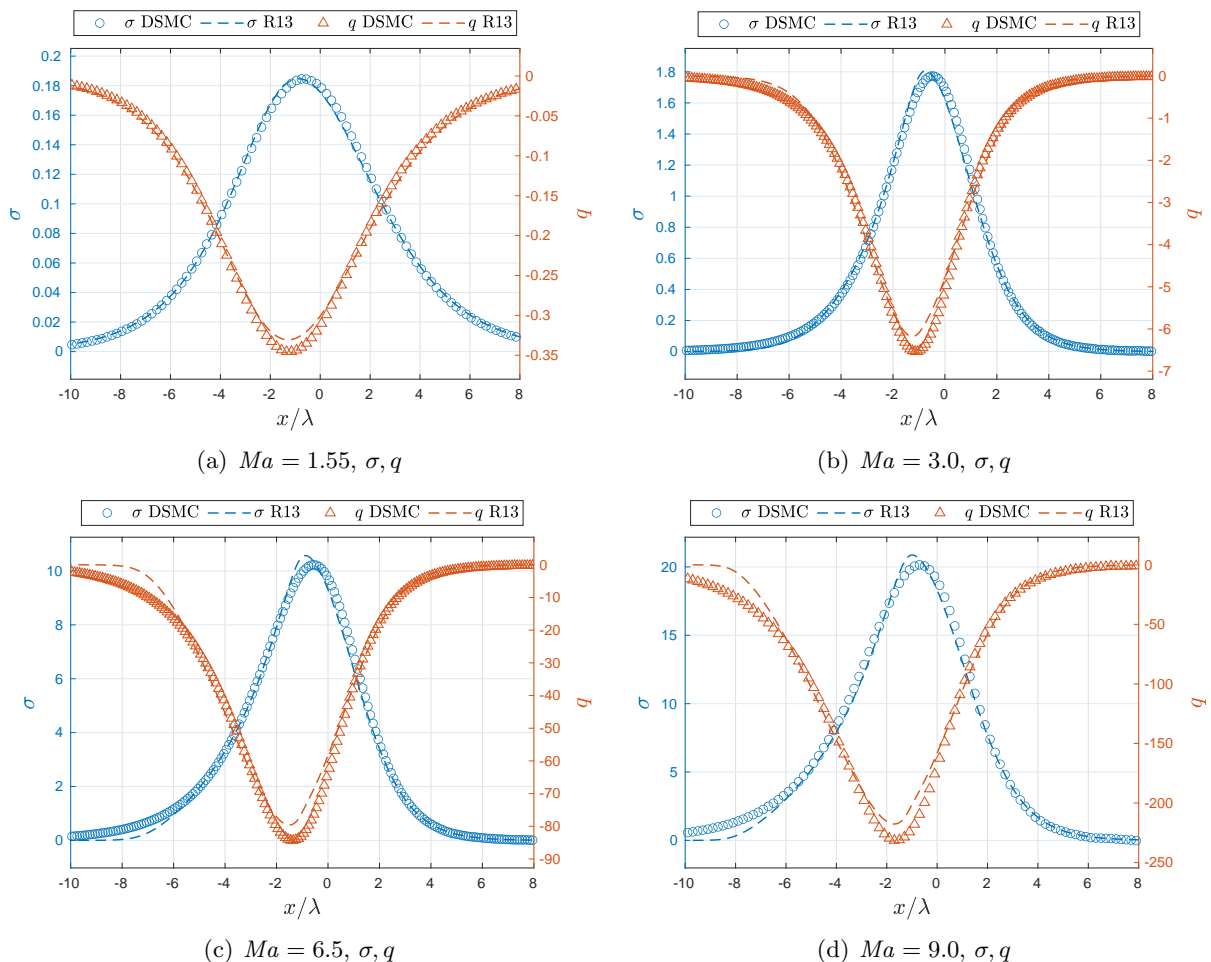


Figure 8: The stress σ and heat flux q of shock structures for the IPL model with $\eta = 10$ and Mach numbers $Ma = 1.55, 3, 6.5, 9$. DSMC results for the variable hard sphere model are provided as references. The horizontal axis is x/λ with λ being the mean free path. The left y -axis corresponds to the stress and the right y -axis corresponds to the heat flux.

Again, the most obvious deviation between R13 and DSMC results appears in the plots of heat fluxes in the low density region. In general, the distribution function inside a shock wave is similar to the superposition of two Maxwellians: a narrow one coming from the front of the shock wave and a wide one from the back of the shock wave [46]. In the low density region, the portion of the wide Maxwellian is quite small. However, when evaluating high-order moments, the contribution of this small portion of wide Maxwellian becomes obvious due to its slow decay at infinity. For the 13-moment approximation, it can be expected that the contribution of the tail may be underestimated, since the decay rate of the distribution function in the Chapman-Enskog expansion is mainly set by the local temperature, which is significantly faster than the wide Maxwellian in the low density region.

As a summary, we observe that R13 models predicts reasonable shock structures both qualitatively and quantitatively, although the derivation of the models does not involve any special consideration for this specific problem. This indicates the potential use of such a model not only for the low Knudsen number case, but also for high speed rarefied gas flows.

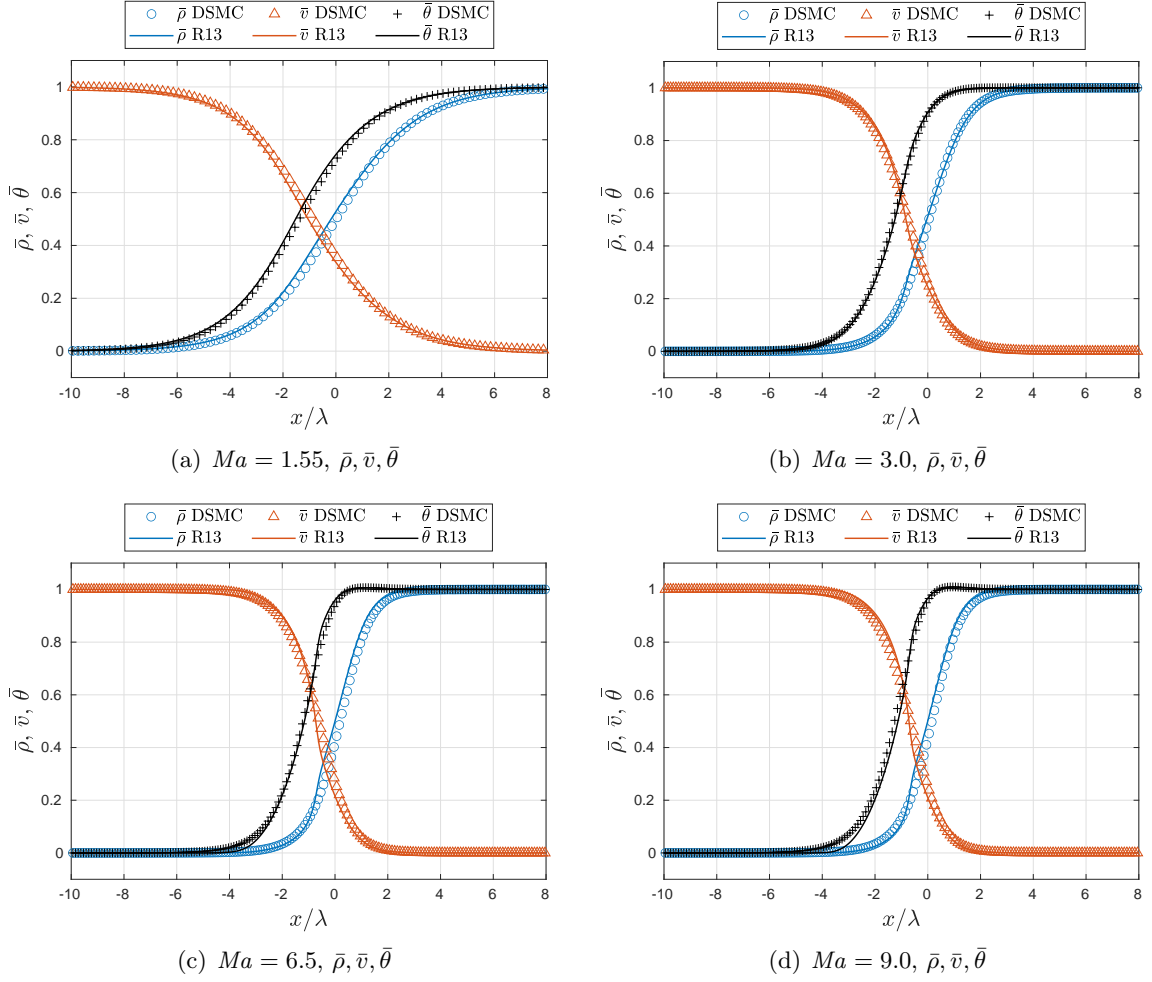


Figure 9: Normalized density, velocity, and temperature of shock structures for the hard-sphere model and Mach numbers $Ma = 1.55, 3, 6.5, 9$. DSMC solutions for the variable hard sphere model are provided as reference results. The horizontal axis is x/λ with λ being the mean free path.

5 Conclusion

In this work, we have derived the regularized 13-moment equations for all inverse power law models and the hard-sphere model. This work can be considered as a generalization of [36] to a much more general class of gas molecules. It also generalizes the methodology of [34], which proposed the derivation of GG13 equations for general collision models, to one more order of accuracy. The derivation follows a systematic routine which can be in principle applied to all collision models. In the numerical experiment for shock structures, these new models show good agreement with the kinetic model in strong nonequilibrium regimes. To better understand how R13 equations describe the distribution functions, one may plot the distribution function predicted by R13 models inside the shock structure, which is to be considered in the future work.

A significant drawback of these models is the high complexity of collision terms, which are given in Appendix C. This may cause difficulties in both understanding the models and designing the numerical methods. One possible way to simplify the equations is to linearize the regularization terms as in [42, 10], which still needs further justification. We are currently

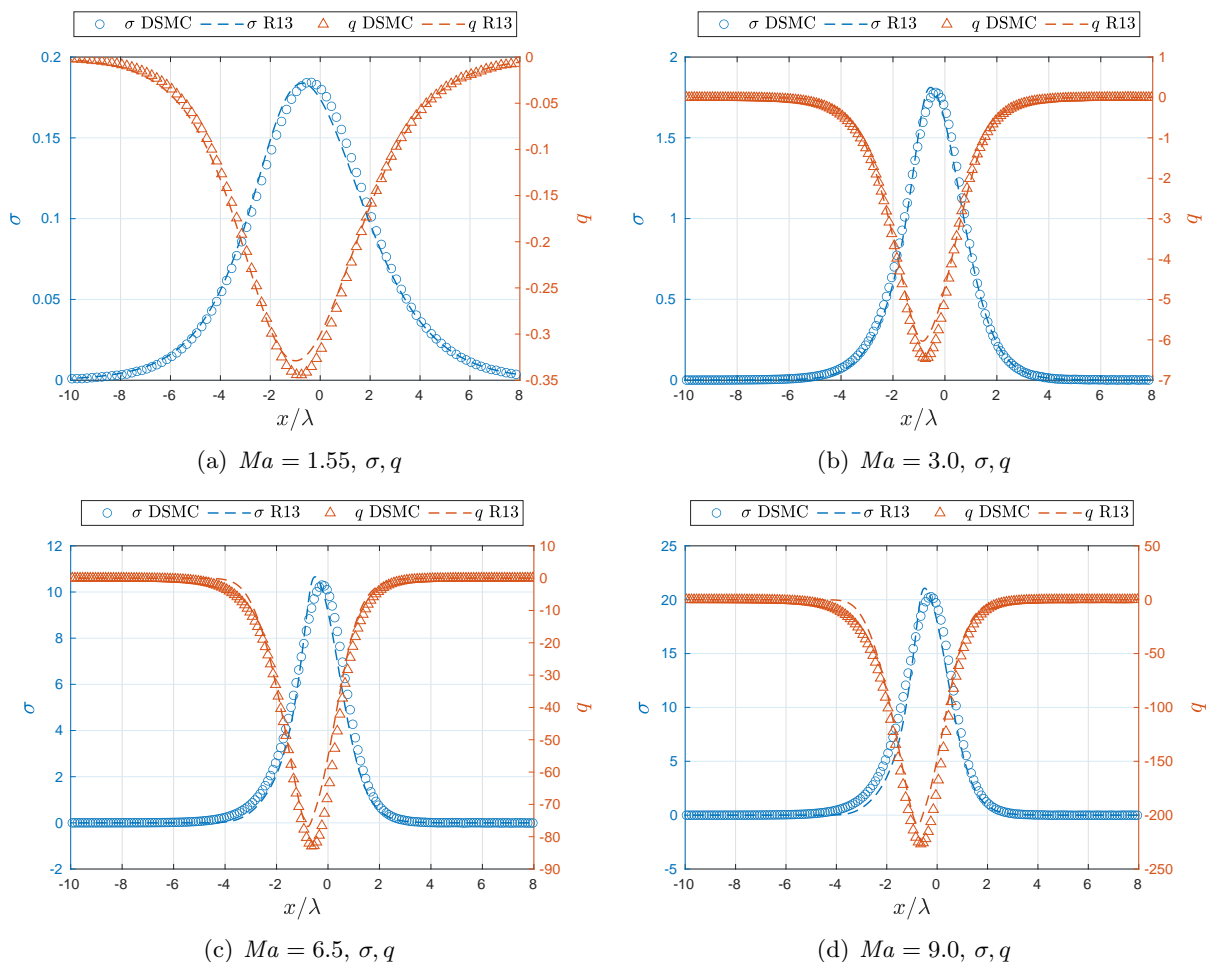


Figure 10: The stress σ and heat flux q of shock structures for the hard-sphere model and Mach numbers $Ma = 1.55, 3, 6.5, 9$. DSMC results for the variable hard sphere model are provided as references. The horizontal axis is x/λ with λ being the mean free path. The left y -axis corresponds to the stress and the right y -axis corresponds to the heat flux.

also working on the derivation of regularized 13-moment equations for Boltzmann equation with binary collision terms.

Acknowledgements

Zhenning Cai is supported by National University of Singapore Startup Fund under Grant No. R-146-000-241-133. Yanli Wang is supported by the National Natural Scientific Foundation of China (Grant No. 91630310 and U1930402).

A Introduction to the Boltzmann equation and the linearized IPL model

As introduced in the beginning of Section 3, both GG13 equations and R13 equations are derived from the kinetic equation, which governs the distribution function $f(\mathbf{x}, \boldsymbol{\xi}, t)$. The relation

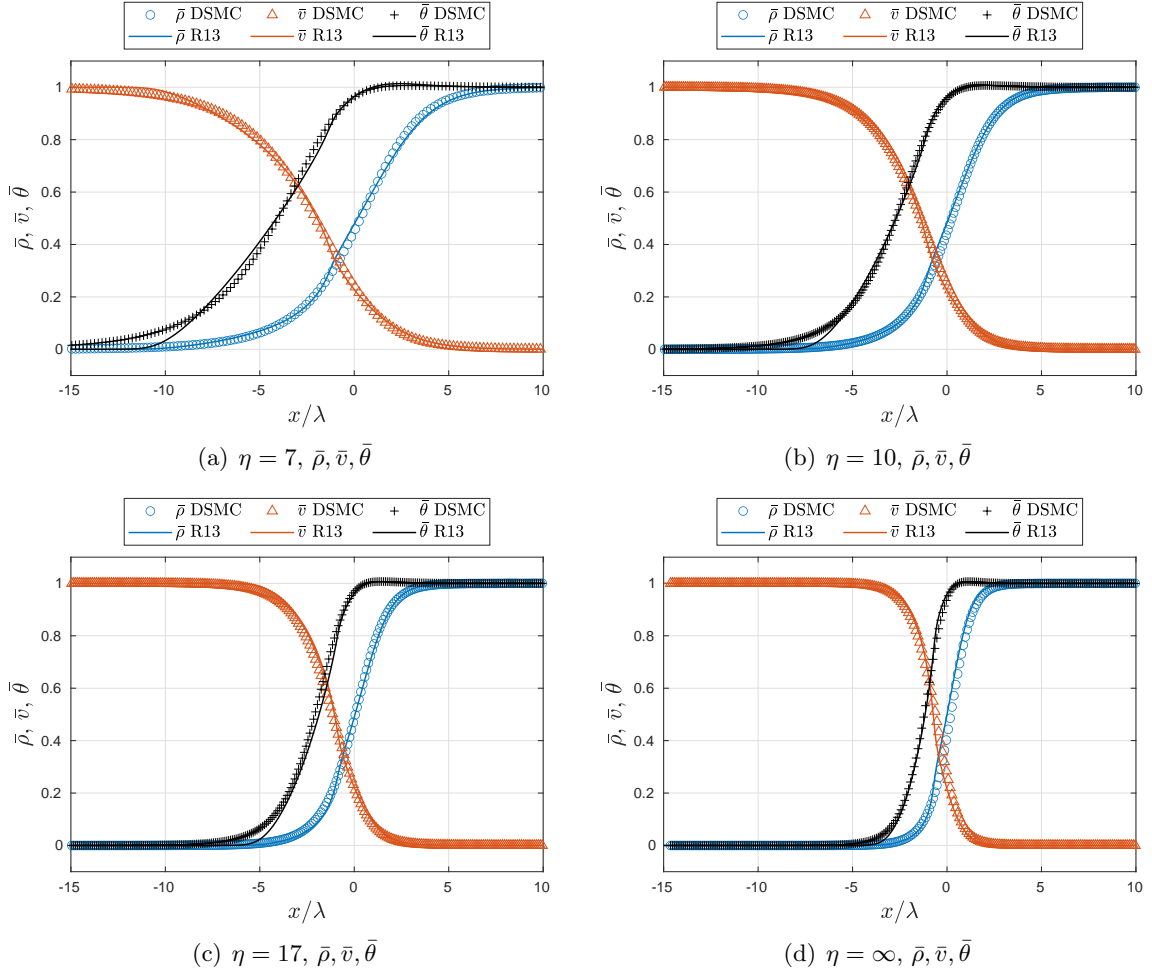


Figure 11: Normalized density, velocity, and temperature of shock structures for IPL models with $\eta = 7, 10, 17, \infty$ (hard-sphere) and Mach numbers $Ma = 6.5$. DSMC solutions for the variable hard sphere models are provided as reference results. The horizontal axis is x/λ with λ being the mean free path.

between the distribution function and the moments has been demonstrated in equations (3.1) and (3.2). An equivalent but more straightforward way to write down the relationship is the follows:

$$\begin{aligned}
 \rho(\mathbf{x}, t) &= m \int_{\mathbb{R}^3} f(\mathbf{x}, \boldsymbol{\xi}, t) d\boldsymbol{\xi}, \\
 \mathbf{v}(\mathbf{x}, t) &= \frac{m}{\rho(\mathbf{x}, t)} \int_{\mathbb{R}^3} \boldsymbol{\xi} f(\mathbf{x}, \boldsymbol{\xi}, t) d\boldsymbol{\xi}, \\
 \theta(\mathbf{x}, t) &= \frac{m}{3\rho(\mathbf{x}, t)} \int_{\mathbb{R}^3} |\boldsymbol{\xi} - \mathbf{v}(\mathbf{x}, t)|^2 f(\mathbf{x}, \boldsymbol{\xi}, t) d\boldsymbol{\xi}, \\
 q_i(\mathbf{x}, t) &= \frac{m}{2} \int_{\mathbb{R}^3} |\boldsymbol{\xi} - \mathbf{v}(\mathbf{x}, t)|^2 (\xi_i - v_i(\mathbf{x}, t)) f(\mathbf{x}, \boldsymbol{\xi}, t) d\boldsymbol{\xi}, \quad i = 1, 2, 3, \\
 \sigma_{ij}(\mathbf{x}, t) &= m \int_{\mathbb{R}^3} \left((\xi_i - v_i(\mathbf{x}, t))(\xi_j - v_j(\mathbf{x}, t)) - \frac{1}{3} \delta_{ij} |\boldsymbol{\xi} - \mathbf{v}(\mathbf{x}, t)|^2 \right) f(\mathbf{x}, \boldsymbol{\xi}, t) d\boldsymbol{\xi}, \quad i, j = 1, 2, 3,
 \end{aligned}
 \tag{A.1}$$

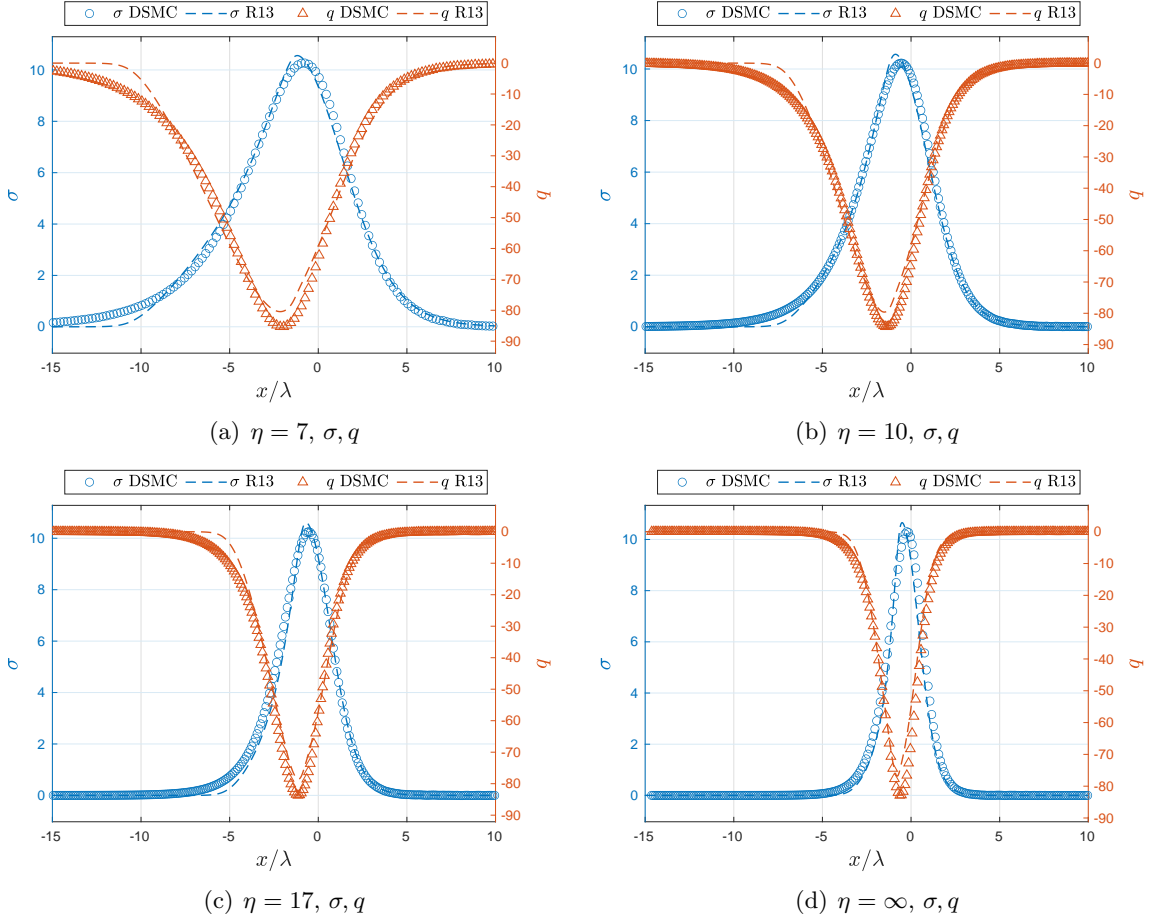


Figure 12: The stress σ and heat flux q of shock structures for IPL models with $\eta = 7, 10, 17, \infty$ (hard-sphere) and Mach numbers $Ma = 6.5$. DSMC results for the variable hard sphere models are provided as references. The horizontal axis is x/λ with λ being the mean free path. The left y -axis corresponds to the stress and the right y -axis corresponds to the heat flux.

where \mathbf{m} is the mass of a single molecule. For monatomic gases, the governing equation of the distribution function is the Boltzmann equation, which reads

$$\frac{\partial f}{\partial t} + \boldsymbol{\xi} \cdot \nabla_{\mathbf{x}} f = C[f], \quad (\text{A.2})$$

where $C(f)$ is the collision term. Here we only focus on the linearized collision term, whose expression is [21]

$$C[f](\mathbf{x}, \boldsymbol{\xi}, t) = \int_{\mathbb{R}^3} \int_{\mathbf{n} \perp \mathbf{g}} B(\mathbf{g}, \chi) \mathcal{M}(\mathbf{x}, \boldsymbol{\xi}, t) \mathcal{M}(\mathbf{x}, \boldsymbol{\xi}_1, t) \times \left[\frac{f(\mathbf{x}, \boldsymbol{\xi}'_1, t)}{\mathcal{M}(\mathbf{x}, \boldsymbol{\xi}'_1, t)} + \frac{f(\mathbf{x}, \boldsymbol{\xi}', t)}{\mathcal{M}(\mathbf{x}, \boldsymbol{\xi}', t)} - \frac{f(\mathbf{x}, \boldsymbol{\xi}_1, t)}{\mathcal{M}(\mathbf{x}, \boldsymbol{\xi}_1, t)} - \frac{f(\mathbf{x}, \boldsymbol{\xi}, t)}{\mathcal{M}(\mathbf{x}, \boldsymbol{\xi}, t)} \right] d\chi d\mathbf{n} d\boldsymbol{\xi}_1, \quad (\text{A.3})$$

where $\mathcal{M}(\mathbf{x}, \boldsymbol{\xi}, t)$ is the local Maxwellian:

$$\mathcal{M}(\mathbf{x}, \boldsymbol{\xi}, t) = \frac{\rho(\mathbf{x}, t)}{\mathbf{m}(2\pi\theta(\mathbf{x}, t))^{3/2}} \exp\left(-\frac{|\boldsymbol{\xi} - \mathbf{v}(\mathbf{x}, t)|^2}{2\theta(\mathbf{x}, t)}\right), \quad (\text{A.4})$$

which satisfies $C[\mathcal{M}] = 0$. In (A.3), $\mathbf{g} = \boldsymbol{\xi} - \boldsymbol{\xi}_1$ and \mathbf{n} is a unit vector. The post-collisional velocities $\boldsymbol{\xi}'$ and $\boldsymbol{\xi}'_1$ are

$$\begin{aligned}\boldsymbol{\xi}' &= \cos^2(\chi/2)\boldsymbol{\xi} + \sin^2(\chi/2)\boldsymbol{\xi}_1 - |\mathbf{g}| \cos(\chi/2) \sin(\chi/2)\mathbf{n}, \\ \boldsymbol{\xi}'_1 &= \cos^2(\chi/2)\boldsymbol{\xi}_1 + \sin^2(\chi/2)\boldsymbol{\xi} + |\mathbf{g}| \cos(\chi/2) \sin(\chi/2)\mathbf{n}.\end{aligned}\tag{A.5}$$

By now, the only unexplained term in the collision term (A.3) is the collision kernel $B(|\mathbf{g}|, \chi)$, which is a non-negative function determined by the force between gas molecules. For the IPL model, it has the form [3]

$$B(|\mathbf{g}|, \chi) = \left(\frac{2\kappa}{\mathbf{m}}\right)^{\frac{2}{\eta-1}} |\mathbf{g}|^{\frac{\eta-5}{\eta-1}} W_0 \left| \frac{dW_0}{d\chi} \right|,\tag{A.6}$$

where η is the same as the parameter used throughout this paper. The dimensionless impact parameter W_0 is related to the angle χ by the following two equations:

$$\chi = \pi - 2 \int_0^{W_1} \left[1 - W^2 - \frac{2}{\eta-1} \left(\frac{W}{W_0}\right)^{\eta-1} \right]^{-1/2} dW, \quad 1 - W_1^2 - \frac{2}{\eta-1} \left(\frac{W_1}{W_0}\right)^{\eta-1} = 0.$$

We also refer the readers to [35] for more information on the Boltzmann equation and the collision models.

B Basis functions and moment equations

In this appendix, we are going to explain the basis functions used in the expansion (3.1) and the terms in the moment equations (3.4). Here we follow [11] to define the basis function $\psi_{lmn}(\mathbf{x}, \boldsymbol{\xi}, t)$ as

$$\psi_{lmn}(\mathbf{x}, \boldsymbol{\xi}, t) = [\theta(\mathbf{x}, t)]^{-\frac{2n+l}{2}} p_{lmn} \left(\frac{\boldsymbol{\xi} - \mathbf{v}(\mathbf{x}, t)}{\sqrt{\theta(\mathbf{x}, t)}} \right) \cdot [2\pi\theta(\mathbf{x}, t)]^{-3/2} \exp\left(-\frac{|\boldsymbol{\xi} - \mathbf{v}(\mathbf{x}, t)|^2}{2\theta(\mathbf{x}, t)}\right),\tag{B.1}$$

where $p_{lmn}(\cdot)$ is an orthogonal polynomial in \mathbb{R}^3 :

$$p_{lmn}(\boldsymbol{\xi}) = \sqrt{\frac{2^{1-l}\pi^{3/2}n!}{\Gamma(n+l+3/2)}} L_n^{(l+1/2)}\left(\frac{|\boldsymbol{\xi}|^2}{2}\right) |\boldsymbol{\xi}|^l Y_l^m\left(\frac{\boldsymbol{\xi}}{|\boldsymbol{\xi}|}\right), \quad l, n \in \mathbb{N}, \quad m = -l, \dots, l,$$

where we have used Laguerre polynomials

$$L_n^{(\alpha)}(x) = \frac{x^{-\alpha} \exp(x)}{n!} \frac{d^n}{dx^n} [x^{n+\alpha} \exp(-x)],\tag{B.2}$$

and spherical harmonics

$$Y_l^m(\mathbf{n}) = \sqrt{\frac{2l+1}{4\pi} \frac{(l-m)!}{(l+m)!}} P_l^m(\cos\theta) \exp(im\phi), \quad \mathbf{n} = (\sin\theta \cos\phi, \sin\theta \sin\phi, \cos\theta)^T$$

with P_l^m being the associate Legendre polynomial:

$$P_l^m(x) = \frac{(-1)^m}{2^l l!} (1-x^2)^{m/2} \frac{d^{l+m}}{dx^{l+m}} [(x^2-1)^l].$$

The orthogonality of the polynomials p_{lmn} is

$$\frac{1}{(2\pi)^{3/2}} \int_{\mathbb{R}^3} \overline{p_{l_1 m_1 n_1}(\boldsymbol{\xi})} p_{l_2 m_2 n_2}(\boldsymbol{\xi}) \exp\left(-\frac{|\boldsymbol{\xi}|^2}{2}\right) d\boldsymbol{\xi} = \delta_{l_1 l_2} \delta_{m_1 m_2} \delta_{n_1 n_2}.$$

Next, we will show the expressions of S_{lmn} and T_{lmn} in (3.4), which have been obtained in [12]. For simplicity, we introduce the following velocities:

$$V_{-1} = \frac{1}{2}(v_1 - iv_2), \quad V_0 = v_3, \quad V_1 = -\frac{1}{2}(v_1 + iv_2). \quad (\text{B.3})$$

Then we have

$$\begin{aligned} S_{lmn} = & -\sqrt{n(n+l+1/2)} \frac{\partial \theta}{\partial t} f_{l,m,n-1} \\ & + \sqrt{2} \sum_{\mu=-1}^1 \frac{\partial V_\mu}{\partial t} \left[(-1)^\mu \sqrt{n+l+1/2} \gamma_{l,m+\mu}^{-\mu} f_{l-1,m+\mu,n} - \sqrt{n} \gamma_{-l-1,m+\mu}^{-\mu} f_{l+1,m+\mu,n-1} \right], \end{aligned} \quad (\text{B.4})$$

where γ_{lm}^μ are constants defined by

$$\gamma_{lm}^\mu = \sqrt{\frac{[l + (2\delta_{1,\mu} - 1)m + \delta_{1,\mu}][l - (2\delta_{-1,\mu} - 1)m + \delta_{-1,\mu}]}{(2l-1)(2l+1)}}. \quad (\text{B.5})$$

To introduce T_{lmn} , we first define the following operators:

$$\frac{\partial}{\partial X_{-1}} = \frac{\partial}{\partial x_1} + i \frac{\partial}{\partial x_2}, \quad \frac{\partial}{\partial X_0} = \frac{\partial}{\partial x_3}, \quad \frac{\partial}{\partial X_1} = -\frac{\partial}{\partial x_1} + i \frac{\partial}{\partial x_2}, \quad (\text{B.6})$$

using which we can write down T_{lmn} as

$$\begin{aligned} T_{lmn} = & \sum_{\mu=-1}^1 \left(V_\mu F_{lmn\mu} + \frac{1}{2|\mu|} \left[\sqrt{2(n+l)+1} \gamma_{l,m-\mu}^\mu \theta F_{l-1,m-\mu,n,\mu} - \sqrt{2(n+1)} \gamma_{l,m-\mu}^\mu F_{l-1,m-\mu,n+1,\mu} \right. \right. \\ & \left. \left. + (-1)^\mu \gamma_{-l-1,m-\mu}^\mu (\sqrt{2(n+l)+3} F_{l+1,m-\mu,n,\mu} - \sqrt{2n} \theta F_{l+1,m-\mu,n-1,\mu}) \right] \right), \end{aligned} \quad (\text{B.7})$$

where

$$\begin{aligned} F_{lmn\mu} = & \frac{\partial f_{lmn}}{\partial X_\mu} - \sqrt{n(n+l+1/2)} \frac{\partial \theta}{\partial X_\mu} f_{l,m,n-1} \\ & + \sqrt{2} \sum_{\nu=-1}^1 \frac{\partial V_\nu}{\partial X_\mu} \left[(-1)^\nu \sqrt{n+l+1/2} \gamma_{l,m+\nu}^{-\nu} f_{l-1,m+\nu,n} - \sqrt{n} \gamma_{-l-1,m+\nu}^{-\nu} f_{l+1,m+\nu,n-1} \right]. \end{aligned} \quad (\text{B.8})$$

C R13 collision terms

In this section, we provide the explicit forms of $\Sigma_{ij}^{(\eta,2)}$ and $Q_i^{(\eta,2)}$ and tabulate some values of the coefficients for some choices of η . In the expressions (C.1) and (C.2), $\Xi_k^{(\eta)}$ and $\Lambda_k^{(\eta)}$ are constants depending only on η , whose values are given in Table 6 and 7. These tables are to be read horizontally. For example, in Table 6, the row below “ $\eta = 10$ ” gives the values of $\Xi_0^{(10)}, \Xi_1^{(10)}, \dots, \Xi_9^{(10)}$, and the next row gives the values of $\Xi_{10}^{(10)}, \Xi_{11}^{(10)}, \dots, \Xi_{19}^{(10)}$.

$$\begin{aligned}
\Sigma_{ij}^{(\eta,2)} = & \Xi_0^{(\eta)} \frac{\rho\theta}{\mu} \sigma_{ij} + \Xi_1^{(\eta)} \left(\frac{\partial v_{\langle i} \sigma_{j\rangle k}}{\partial x_k} + \frac{\partial v_k \sigma_{j\rangle k}}{\partial x_{\langle i}} \right) + \Xi_2^{(\eta)} \frac{\partial v_k \sigma_{ij}}{\partial x_k} + \Xi_3^{(\eta)} \frac{\mu}{\rho} \frac{\partial \ln \theta}{\partial x_k} \frac{\partial \ln \theta}{\partial x_{\langle i}} \sigma_{j\rangle k} \\
& + \Xi_4^{(\eta)} \frac{\partial \ln \theta}{\partial x_k} \frac{\partial \ln \theta}{\partial x_k} \sigma_{ij} + \Xi_5^{(\eta)} \frac{\mu}{\rho} \frac{\partial \ln \rho}{\partial x_k} \frac{\partial \ln \theta}{\partial x_{\langle i}} \sigma_{j\rangle k} + \Xi_6^{(\eta)} \frac{\partial \ln \rho}{\partial x_k} \frac{\partial \ln \theta}{\partial x_k} \sigma_{ij} + \Xi_7^{(\eta)} \frac{\mu}{\rho} \frac{\partial \ln \theta}{\partial x_k} \frac{\partial \ln \rho}{\partial x_{\langle i}} \sigma_{j\rangle k} \\
& + \Xi_8^{(\eta)} \frac{\mu}{\rho} \frac{\partial \ln \rho}{\partial x_k} \frac{\partial \ln \rho}{\partial x_{\langle i}} \sigma_{j\rangle k} + \Xi_9^{(\eta)} \frac{\partial \ln \rho}{\partial x_k} \frac{\partial \ln \rho}{\partial x_k} \sigma_{ij} + \Xi_{10}^{(\eta)} \frac{\mu}{\rho\theta} \frac{\partial v_k}{\partial x_l} \frac{\partial v_k}{\partial x_{\langle i}} \sigma_{j\rangle l} + \Xi_{11}^{(\eta)} \frac{\mu}{\rho\theta} \frac{\partial v_k}{\partial x_l} \frac{\partial v_k}{\partial x_l} \sigma_{ij} \\
& + \Xi_{12}^{(\eta)} \frac{\mu}{\rho\theta} \frac{\partial v_k}{\partial x_l} \frac{\partial v_l}{\partial x_k} \sigma_{ij} + \Xi_{13}^{(\eta)} \frac{\mu}{\rho\theta} \frac{\partial v_k}{\partial x_k} \frac{\partial v_l}{\partial x_l} \sigma_{ij} + \Xi_{14}^{(\eta)} \frac{\mu}{\rho\theta} \left(\frac{\partial v_k}{\partial x_l} \frac{\partial v_{\langle i}}{\partial x_k} + \frac{\partial v_l}{\partial x_k} \frac{\partial v_{\langle i}}{\partial x_{\langle i}} \right) \sigma_{j\rangle l} \\
& + \Xi_{15}^{(\eta)} \frac{\mu}{\rho\theta} \frac{\partial v_k}{\partial x_k} \left(\frac{\partial v_{\langle i}}{\partial x_l} + \frac{\partial v_l}{\partial x_{\langle i}} \right) \sigma_{j\rangle l} + \Xi_{16}^{(\eta)} \frac{\mu}{\rho\theta} \left(\frac{\partial v_k}{\partial x_{\langle i}} \frac{\partial v_l}{\partial x_j} + \frac{\partial v_{\langle i}}{\partial x_k} \frac{\partial v_{j\rangle}}{\partial x_l} \right) \sigma_{kl} \\
& + \Xi_{17}^{(\eta)} \frac{\mu}{\rho\theta} \frac{\partial v_l}{\partial x_{\langle i}} \frac{\partial v_{j\rangle}}{\partial x_k} \sigma_{kl} + \Xi_{18}^{(\eta)} \frac{\partial v_l}{\partial x_k} \frac{\partial v_{\langle i}}{\partial x_k} \sigma_{j\rangle l} + \Xi_{19}^{(\eta)} \frac{\mu}{\rho\theta} \frac{\partial^2 \theta}{\partial x_k \partial x_k} \sigma_{ij} + \Xi_{20}^{(\eta)} \frac{\mu}{\rho\theta} \frac{\partial^2 \theta}{\partial x_k \partial x_{\langle i}} \sigma_{j\rangle k} \\
& + \Xi_{21}^{(\eta)} \frac{\mu}{\rho} \frac{\partial \sigma_{ij}}{\partial x_k} \frac{\partial \ln \theta}{\partial x_k} + \Xi_{22}^{(\eta)} \frac{\mu}{\rho} \frac{\partial \sigma_{k\langle i}}{\partial x_k} \frac{\partial \ln \theta}{\partial x_j} + \Xi_{23}^{(\eta)} \frac{\mu}{\rho} \frac{\partial \sigma_{k\langle i}}{\partial x_j} \frac{\partial \ln \theta}{\partial x_k} + \Xi_{24}^{(\eta)} \frac{\mu}{\rho^2} \frac{\partial^2 \rho}{\partial x_k \partial x_k} \sigma_{ij} \\
& + \Xi_{25}^{(\eta)} \frac{\mu}{\rho^2} \frac{\partial^2 \rho}{\partial x_k \partial x_{\langle i}} \sigma_{j\rangle k} + \Xi_{26}^{(\eta)} \frac{\mu}{\rho} \frac{\partial \sigma_{ij}}{\partial x_k} \frac{\partial \ln \rho}{\partial x_k} + \Xi_{27}^{(\eta)} \frac{\mu}{\rho} \frac{\partial \sigma_{k\langle i}}{\partial x_k} \frac{\partial \ln \rho}{\partial x_j} + \Xi_{28}^{(\eta)} \frac{\mu}{\rho} \frac{\partial \sigma_{k\langle i}}{\partial x_j} \frac{\partial \ln \rho}{\partial x_k} \\
& + \Xi_{29}^{(\eta)} \frac{\mu}{\rho} \frac{\partial^2 \sigma_{ij}}{\partial x_k \partial x_k} + \Xi_{30}^{(\eta)} \frac{\mu}{\rho} \frac{\partial^2 \sigma_{k\langle i}}{\partial x_j \partial x_k} + \Xi_{31}^{(\eta)} \mu \frac{\partial v_{\langle i}}{\partial x_k} \frac{\partial v_{j\rangle}}{\partial x_k} + \Xi_{32}^{(\eta)} \mu \frac{\partial v_k}{\partial x_{\langle i}} \frac{\partial v_k}{\partial x_j} + \Xi_{33}^{(\eta)} \mu \frac{\partial v_{\langle i}}{\partial x_k} \frac{\partial v_k}{\partial x_j} \\
& + \Xi_{34}^{(\eta)} \mu \frac{\partial v_k}{\partial x_k} \frac{\partial v_{\langle i}}{\partial x_j} + \Xi_{35}^{(\eta)} \rho\theta \frac{\partial v_{\langle i}}{\partial x_j} + \Xi_{36}^{(\eta)} \mu\theta \frac{\partial \ln \theta}{\partial x_{\langle i}} \frac{\partial \ln \theta}{\partial x_j} + \Xi_{37}^{(\eta)} \mu\theta \frac{\partial \ln \rho}{\partial x_{\langle i}} \frac{\partial \ln \rho}{\partial x_j} + \Xi_{38}^{(\eta)} \mu\theta \frac{\partial \ln \rho}{\partial x_{\langle i}} \frac{\partial \ln \theta}{\partial x_j} \\
& + \Xi_{39}^{(\eta)} \frac{\mu}{\rho\theta} \frac{\partial v_k}{\partial x_k} \frac{\partial \ln \theta}{\partial x_{\langle i}} q_{j\rangle} + \Xi_{40}^{(\eta)} \frac{\mu}{\rho\theta} \frac{\partial v_{\langle i}}{\partial x_k} \frac{\partial \ln \theta}{\partial x_j} q_k + \Xi_{41}^{(\eta)} \frac{\mu}{\rho\theta} \frac{\partial \ln \theta}{\partial x_k} \frac{\partial v_{\langle i}}{\partial x_k} q_{j\rangle} + \Xi_{42}^{(\eta)} \frac{\mu}{\rho\theta} \frac{\partial \ln \theta}{\partial x_k} \frac{\partial v_k}{\partial x_{\langle i}} q_{j\rangle} \\
& + \Xi_{43}^{(\eta)} \frac{\mu}{\rho\theta} \frac{\partial \ln \theta}{\partial x_{\langle i}} \frac{\partial v_k}{\partial x_j} q_k + \Xi_{44}^{(\eta)} \frac{\mu}{\rho\theta} \frac{\partial \ln \theta}{\partial x_k} \frac{\partial v_{\langle i}}{\partial x_j} q_k + \Xi_{45}^{(\eta)} \frac{\mu}{\rho\theta} \frac{\partial v_k}{\partial x_k} \frac{\partial \ln \rho}{\partial x_{\langle i}} q_{j\rangle} + \Xi_{46}^{(\eta)} \frac{\mu}{\rho\theta} \frac{\partial v_{\langle i}}{\partial x_k} \frac{\partial \ln \rho}{\partial x_j} q_k \\
& + \Xi_{47}^{(\eta)} \frac{\mu}{\rho\theta} \frac{\partial \ln \rho}{\partial x_k} \frac{\partial v_{\langle i}}{\partial x_k} q_{j\rangle} + \Xi_{48}^{(\eta)} \frac{\mu}{\rho\theta} \frac{\partial \ln \rho}{\partial x_k} \frac{\partial v_k}{\partial x_{\langle i}} q_{j\rangle} + \Xi_{49}^{(\eta)} \frac{\mu}{\rho\theta} \frac{\partial v_{\langle i}}{\partial x_k} \frac{\partial \ln \rho}{\partial x_j} q_k + \Xi_{50}^{(\eta)} \frac{\mu}{\rho\theta} \frac{\partial \ln \rho}{\partial x_k} \frac{\partial v_{\langle i}}{\partial x_j} q_k \\
& + \Xi_{51}^{(\eta)} \frac{\mu}{\rho\theta} \frac{\partial q_{\langle i}}{\partial x_k} \frac{\partial v_{j\rangle}}{\partial x_k} + \Xi_{52}^{(\eta)} \frac{\mu}{\rho\theta} \frac{\partial q_{\langle i}}{\partial x_k} \frac{\partial v_k}{\partial x_j} + \Xi_{53}^{(\eta)} \frac{\mu}{\rho\theta} \left(\frac{\partial q_k}{\partial x_{\langle i}} \frac{\partial v_k}{\partial x_j} + \frac{\partial q_k}{\partial x_{\langle i}} \frac{\partial v_{j\rangle}}{\partial x_k} \right) + \Xi_{54}^{(\eta)} \frac{\mu}{\rho\theta} \frac{\partial q_k}{\partial x_k} \frac{\partial v_{\langle i}}{\partial x_j} \\
& + \Xi_{55}^{(\eta)} \frac{\mu}{\rho\theta} \frac{\partial q_{\langle i}}{\partial x_j} \frac{\partial v_k}{\partial x_k} + \Xi_{56}^{(\eta)} \frac{\mu}{\rho\theta} \frac{\partial^2 v_{\langle i}}{\partial x_k \partial x_k} q_{j\rangle} + \Xi_{57}^{(\eta)} \frac{\mu}{\rho\theta} \frac{\partial^2 v_k}{\partial x_k \partial x_{\langle i}} q_{j\rangle} + \Xi_{58}^{(\eta)} \frac{\mu}{\rho\theta} \frac{\partial^2 v_k}{\partial x_{\langle i} \partial x_j} q_k \\
& + \Xi_{59}^{(\eta)} \frac{\mu}{\rho\theta} \frac{\partial^2 v_{\langle i}}{\partial x_j \partial x_k} q_k + \Xi_{60}^{(\eta)} q_{\langle i} \frac{\partial \ln \theta}{\partial x_j} + \Xi_{61}^{(\eta)} \frac{\partial^2 v_{\langle i}}{\partial x_j \partial x_k} q_k + \Xi_{62}^{(\eta)} \frac{\mu \partial^2 \theta}{\partial x_{\langle i} \partial x_j} + \Xi_{63}^{(\eta)} \frac{\partial q_{\langle i}}{\partial x_j} + \Xi_{64}^{(\eta)} \frac{\mu\theta}{\rho} \frac{\partial^2 \rho}{\partial x_{\langle i} \partial x_j} \\
& + \frac{1}{\rho\theta} \left(\Xi_{65}^{(\eta)} \sigma_{ij} \frac{\partial q_k}{\partial x_k} + \Xi_{66}^{(\eta)} \sigma_{ij} \frac{\partial v_k}{\partial x_l} \sigma_{kl} \right).
\end{aligned} \tag{C.1}$$

$$\begin{aligned}
Q_i^{(\eta,2)} = & \Lambda_0^{(\eta)} \frac{\theta \rho}{\mu} q_i + \Lambda_1^{(\eta)} \sigma_{ik} \frac{\partial \theta}{\partial x_k} + \Lambda_2^{(\eta)} \frac{\mu}{\rho} q_i \frac{\partial \ln \theta}{\partial x_k} \frac{\partial \ln \theta}{\partial x_k} + \Lambda_3^{(\eta)} \frac{\mu}{\rho} q_k \frac{\partial \ln \theta}{\partial x_k} \frac{\partial \ln \theta}{\partial x_i} + \Lambda_4^{(\eta)} \theta \sigma_{ik} \frac{\partial \ln \rho}{\partial x_k} + \Lambda_5^{(\eta)} \frac{\mu}{\rho} q_k \frac{\partial \ln \rho}{\partial x_k} \frac{\partial \ln \theta}{\partial x_i} \\
& + \Lambda_6^{(\eta)} \frac{\mu}{\rho} q_k \frac{\partial \ln \rho}{\partial x_i} \frac{\partial \ln \theta}{\partial x_k} + \Lambda_7^{(\eta)} \frac{\mu}{\rho} q_i \frac{\partial \ln \rho}{\partial x_k} \frac{\partial \ln \theta}{\partial x_k} + \Lambda_8^{(\eta)} \frac{\mu}{\rho} q_i \frac{\partial \ln \rho}{\partial x_k} \frac{\partial \ln \rho}{\partial x_k} + \Lambda_9^{(\eta)} \frac{\mu}{\rho} q_k \frac{\partial \ln \rho}{\partial x_k} \frac{\partial \ln \rho}{\partial x_i} + \Lambda_{10}^{(\eta)} \frac{\mu}{\rho} \frac{\partial \ln \theta}{\partial x_i} \frac{\partial q_k}{\partial x_k} \\
& + \Lambda_{11}^{(\eta)} \frac{\mu}{\rho} \frac{\partial \ln \theta}{\partial x_k} \frac{\partial q_i}{\partial x_k} + \Lambda_{12}^{(\eta)} \frac{\mu}{\rho} \frac{\partial \ln \theta}{\partial x_k} \frac{\partial q_k}{\partial x_i} + \Lambda_{13}^{(\eta)} \frac{\mu}{\rho} \frac{\partial \rho}{\partial x_i} \frac{\partial q_k}{\partial x_k} + \Lambda_{14}^{(\eta)} \frac{\mu}{\rho} \frac{\partial \rho}{\partial x_k} \frac{\partial q_i}{\partial x_k} + \Lambda_{15}^{(\eta)} \frac{\mu}{\rho} \frac{\partial \rho}{\partial x_k} \frac{\partial q_k}{\partial x_i} \\
& + \Lambda_{16}^{(\eta)} q_k \left(\frac{\partial v_k}{\partial x_i} + \frac{\partial v_i}{\partial x_k} \right) + \Lambda_{17}^{(\eta)} q_i \frac{\partial v_k}{\partial x_k} + \Lambda_{18}^{(\eta)} \mu \frac{\partial \theta}{\partial x_k} \frac{\partial v_k}{\partial x_i} + \Lambda_{19}^{(\eta)} \mu \frac{\partial \theta}{\partial x_k} \frac{\partial v_i}{\partial x_k} + \Lambda_{20}^{(\eta)} \mu \frac{\partial \theta}{\partial x_i} \frac{\partial v_k}{\partial x_k} \\
& + \Lambda_{21}^{(\eta)} \frac{\mu}{\rho} \sigma_{kl} \left(\frac{\partial \ln \theta}{\partial x_k} \frac{\partial v_i}{\partial x_l} + \frac{\partial \ln \theta}{\partial x_l} \frac{\partial v_i}{\partial x_k} + \frac{\partial \ln \theta}{\partial x_k} \frac{\partial v_k}{\partial x_i} \right) + \Lambda_{22}^{(\eta)} \frac{\mu}{\rho} \sigma_{kl} \left(\frac{\partial \ln \theta}{\partial x_i} \frac{\partial v_l}{\partial x_k} + \frac{\partial \ln \theta}{\partial x_i} \frac{\partial v_k}{\partial x_l} \right) \\
& + \Lambda_{23}^{(\eta)} \frac{\mu}{\rho} \sigma_{il} \frac{\partial \ln \theta}{\partial x_k} \frac{\partial v_l}{\partial x_k} + \Lambda_{24}^{(\eta)} \frac{\mu}{\rho} \sigma_{il} \frac{\partial \ln \theta}{\partial x_k} \frac{\partial v_k}{\partial x_l} + \Lambda_{25}^{(\eta)} \frac{\mu}{\rho} \sigma_{il} \frac{\partial \ln \theta}{\partial x_l} \frac{\partial v_k}{\partial x_k} + \Lambda_{26}^{(\eta)} \mu \theta \frac{\partial \ln \rho}{\partial x_i} \frac{\partial v_k}{\partial x_k} \\
& + \Lambda_{27}^{(\eta)} \mu \theta \left(\frac{\partial \ln \rho}{\partial x_k} \frac{\partial v_i}{\partial x_k} + \frac{\partial \ln \rho}{\partial x_k} \frac{\partial v_k}{\partial x_i} \right) + \Lambda_{28}^{(\eta)} \frac{\mu}{\rho} \sigma_{kl} \left(\frac{\partial \ln \rho}{\partial x_k} \frac{\partial v_i}{\partial x_l} + \frac{\partial \ln \rho}{\partial x_l} \frac{\partial v_i}{\partial x_k} + \frac{\partial \ln \rho}{\partial x_k} \frac{\partial v_l}{\partial x_i} + \frac{\partial \ln \rho}{\partial x_l} \frac{\partial v_k}{\partial x_i} \right) \\
& + \Lambda_{29}^{(\eta)} \frac{\mu}{\rho} \sigma_{kl} \left(\frac{\partial \ln \rho}{\partial x_i} \frac{\partial v_l}{\partial x_k} + \frac{\partial \ln \rho}{\partial x_i} \frac{\partial v_k}{\partial x_l} \right) + \Lambda_{30}^{(\eta)} \frac{\mu}{\rho} \sigma_{il} \frac{\partial \ln \rho}{\partial x_k} \frac{\partial v_l}{\partial x_k} + \Lambda_{31}^{(\eta)} \frac{\mu}{\rho} \sigma_{il} \frac{\partial \ln \rho}{\partial x_k} \frac{\partial v_k}{\partial x_l} + \Lambda_{32}^{(\eta)} \frac{\mu}{\rho} \sigma_{il} \frac{\partial \ln \rho}{\partial x_l} \frac{\partial v_k}{\partial x_k} \\
& + \Lambda_{33}^{(\eta)} \frac{\mu}{\rho \theta} q_i \frac{\partial v_k}{\partial x_k} \frac{\partial v_l}{\partial x_l} + \Lambda_{34}^{(\eta)} \frac{\mu}{\rho \theta} q_i \frac{\partial v_k}{\partial x_l} \frac{\partial v_k}{\partial x_l} + \Lambda_{35}^{(\eta)} \frac{\mu}{\rho \theta} q_i \frac{\partial v_k}{\partial x_l} \frac{\partial v_l}{\partial x_k} + \Lambda_{36}^{(\eta)} \frac{\mu}{\rho \theta} q_k \left(\frac{\partial v_k}{\partial x_i} \frac{\partial v_l}{\partial x_l} + \frac{\partial v_i}{\partial x_k} \frac{\partial v_l}{\partial x_l} \right) \\
& + \Lambda_{37}^{(\eta)} \frac{\mu}{\rho \theta} q_k \frac{\partial v_k}{\partial x_l} \frac{\partial v_i}{\partial x_l} + \Lambda_{38}^{(\eta)} \frac{\mu}{\rho \theta} q_k \left(\frac{\partial v_k}{\partial x_l} \frac{\partial v_l}{\partial x_i} + \frac{\partial v_l}{\partial x_k} \frac{\partial v_i}{\partial x_l} + \frac{\partial v_l}{\partial x_k} \frac{\partial v_l}{\partial x_i} \right) + \Lambda_{39}^{(\eta)} \frac{\mu}{\rho} \frac{\partial v_k}{\partial x_k} \frac{\partial \sigma_{il}}{\partial x_l} + \Lambda_{40}^{(\eta)} \frac{\mu}{\rho} \frac{\partial v_l}{\partial x_k} \frac{\partial \sigma_{il}}{\partial x_k} \\
& + \Lambda_{41}^{(\eta)} \frac{\mu}{\rho} \frac{\partial v_k}{\partial x_l} \frac{\partial \sigma_{il}}{\partial x_k} + \Lambda_{42}^{(\eta)} \frac{\mu}{\rho} \left(\frac{\partial v_k}{\partial x_l} \frac{\partial \sigma_{kl}}{\partial x_i} + \frac{\partial v_l}{\partial x_k} \frac{\partial \sigma_{kl}}{\partial x_i} \right) + \Lambda_{43}^{(\eta)} \frac{\mu}{\rho} \left(\frac{\partial v_i}{\partial x_k} \frac{\partial \sigma_{kl}}{\partial x_l} + \frac{\partial v_k}{\partial x_i} \frac{\partial \sigma_{kl}}{\partial x_l} \right) + \Lambda_{44}^{(\eta)} \frac{\mu}{\rho} \sigma_{il} \frac{\partial^2 v_k}{\partial x_k \partial x_l} \\
& + \Lambda_{45}^{(\eta)} \frac{\mu}{\rho} \sigma_{il} \frac{\partial^2 v_l}{\partial x_k \partial x_k} + \Lambda_{46}^{(\eta)} \frac{\mu}{\rho} \sigma_{kl} \frac{\partial^2 v_i}{\partial x_k \partial x_l} + \Lambda_{47}^{(\eta)} \frac{\mu}{\rho} \sigma_{kl} \frac{\partial^2 v_k}{\partial x_i \partial x_l} + \Lambda_{48}^{(\eta)} \theta \frac{\partial \sigma_{ik}}{\partial x_k} + \Lambda_{49}^{(\eta)} \frac{\mu}{\theta \rho} q_k \frac{\partial^2 \theta}{\partial x_k \partial x_i} \\
& + \Lambda_{50}^{(\eta)} \frac{\mu}{\theta \rho} q_i \frac{\partial^2 \theta}{\partial x_k \partial x_k} + \Lambda_{51}^{(\eta)} \frac{\mu}{\rho^2} q_k \frac{\partial^2 \rho}{\partial x_k \partial x_i} + \Lambda_{52}^{(\eta)} \frac{\mu}{\rho^2} q_i \frac{\partial^2 \rho}{\partial x_k \partial x_k} + \Lambda_{53}^{(\eta)} \frac{\mu}{\rho} \frac{\partial^2 q_i}{\partial x_k \partial x_k} + \Lambda_{54}^{(\eta)} \frac{\mu}{\rho} \frac{\partial^2 q_k}{\partial x_i \partial x_k} \\
& + \Lambda_{55}^{(\eta)} \mu \theta \frac{\partial^2 v_i}{\partial x_k \partial x_k} + \Lambda_{56}^{(\eta)} \mu \theta \frac{\partial^2 v_k}{\partial x_i \partial x_k} + \Lambda_{57}^{(\eta)} \theta \rho \frac{\partial \theta}{\partial x_i} + \frac{1}{\rho} \Lambda_{58}^{(\eta)} \sigma_{ik} \frac{\partial \sigma_{lk}}{\partial x_l} + \frac{q_i}{\theta \rho} \left(\Lambda_{59}^{(\eta)} \frac{\partial q_k}{\partial x_k} + \Lambda_{60}^{(\eta)} \sigma_{lk} \frac{\partial v_l}{\partial x_k} \right). \tag{C.2}
\end{aligned}$$

References

- [1] G. B. Arfken, H. J. Weber, and F. E. Harris. *Mathematical Methods for Physicists (Seventh Edition)*. Academic Press, 2013.
- [2] S. Bayin. *Mathematical Methods in Science and Engineering, Second Edition*. Wiley, 2018.
- [3] G. A. Bird. *Molecular Gas Dynamics and the Direct Simulation of Gas Flows*. Oxford: Clarendon Press, 1994.
- [4] A. V. Bobylev. The Chapman-Enskog and Grad methods for solving the Boltzmann equation. *Sov. Phys. Dokl.*, 27:29–31, 1982.
- [5] A. V. Bobylev. Instabilities in the Chapman-Enskog expansion and hyperbolic Burnett equations. *J. Stat. Phys.*, 124(2–4):371–399, 2006.
- [6] A. V. Bobylev. Generalized Burnett hydrodynamics. *J. Stat. Phys.*, 132:569–580, 2008.

$\eta = 7$									
0.0013	0.0342	-0.0228	-0.0198	-0.0147	0.0096	0.0664	0.0367	-0.0162	-0.0151
0.0092	0.0101	-0.0023	-0.0100	-0.0125	0.0377	-0.0155	-0.0526	-0.0603	-0.0721
0.0435	-0.0973	0.0018	-0.0249	-0.0110	0.0347	0.0378	-0.0450	-0.0077	-0.0120
0.0337	0.0317	0.0344	0.0687	-0.0910	0.0026	0.1587	-0.0026	-0.0002	0.0162
0.0065	-0.0586	-0.0252	0.0065	-0.1879	-0.0121	-0.0109	0.1117	0.0124	-0.0109
0.0968	-0.0927	0.0053	0.0105	-0.1034	0.0003	-0.0500	0.0237	0.0042	0.0032
0.0158	-0.0007	0.1214	0.0326	0.0026	0.0009	0.0009	×	×	×
$\eta = 10$									
0.0037	0.0566	-0.0377	-0.0303	-0.0072	0.0212	0.0981	0.0477	-0.0218	-0.0227
0.0217	0.0139	-0.0071	-0.0074	-0.0140	0.0456	-0.0227	-0.0810	-0.0948	-0.1173
0.0764	-0.1527	-0.0139	-0.0315	-0.0201	0.0554	0.0603	-0.0773	-0.0154	-0.0184
0.0579	0.0497	0.0571	0.1142	-0.1512	0.0074	0.2231	-0.0074	-0.0012	0.0219
0.0080	-0.0634	-0.0380	0.0080	-0.2779	-0.0088	-0.0198	0.1825	0.0143	-0.0198
0.1530	-0.1523	0.0125	0.0171	-0.1582	-0.0075	-0.0808	0.0306	0.0061	0.0076
0.0216	-0.0019	0.2029	0.0543	0.0074	0.0026	0.0026	×	×	×
$\eta = 17$									
0.0068	0.0761	-0.0507	-0.0403	0.0093	0.0358	0.1187	0.0493	-0.0236	-0.0278
0.0368	0.0155	-0.0135	0.0009	-0.0111	0.0417	-0.0271	-0.1022	-0.1221	-0.1564
0.1076	-0.1969	-0.0385	-0.0315	-0.0294	0.0722	0.0786	-0.1081	-0.0239	-0.0231
0.0808	0.0635	0.0774	0.1548	-0.2052	0.0137	0.2536	-0.0139	-0.0032	0.0276
0.0071	-0.0462	-0.0488	0.0071	-0.3379	0.0019	-0.0290	0.2436	0.0116	-0.0290
0.1978	-0.2042	0.0211	0.0227	-0.1987	-0.0198	-0.1069	0.0304	0.0073	0.0130
0.0234	-0.0036	0.2760	0.0736	0.0139	0.0050	0.0050	×	×	×
$\eta = \infty$									
0.0124	0.1016	-0.0677	-0.0574	0.0433	0.0628	0.1364	0.0399	-0.0213	-0.0322
0.0627	0.0152	-0.0250	0.0202	-0.0015	0.0213	-0.0305	-0.1253	-0.1542	-0.2079
0.1511	-0.2502	-0.0861	-0.0239	-0.0438	0.0927	0.1006	-0.1524	-0.0372	-0.0280
0.1134	0.0788	0.1048	0.2096	-0.2794	0.0252	0.2561	-0.0260	-0.0086	0.0414
0.0025	0.0058	-0.0647	0.0025	-0.3929	0.0277	-0.0435	0.3228	0.0020	-0.0435
0.2502	-0.2727	0.0353	0.0302	-0.2419	-0.0437	-0.1405	0.0203	0.0084	0.0220
0.0208	-0.0067	0.3748	0.0988	0.0260	0.0096	0.0096	×	×	×

Table 6: Coefficients $\Xi_i^{(\eta)}$ in (C.1) for different η .

- [7] D. Burnett. The distribution of molecular velocities and the mean motion in a non-uniform gas. *Proc. London Math. Soc.*, 40(1):382–435, 1936.
- [8] Z. Cai, Y. Fan, and R. Li. On hyperbolicity of 13-moment system. *Kin. Rel. Models*, 7(3):415–432, 2014.
- [9] Z. Cai, Y. Fan, and R. Li. A framework on moment model reduction for kinetic equation. *SIAM J. Appl. Math.*, 75(5):2001–2023, 2015.
- [10] Z. Cai, R. Li, and Y. Wang. Numerical regularized moment method for high Mach number flow. *Commun. Comput. Phys.*, 11(5):1415–1438, 2012.
- [11] Z. Cai and M. Torrilhon. Approximation of the linearized Boltzmann collision operator for hard-sphere and inverse-power-law models. *J. Comput. Phys.*, 295:617–643, 2015.
- [12] Z. Cai and M. Torrilhon. Numerical simulation of microflows using moment methods with linearized collision operator. *J. Sci. Comput.*, 74(1):336–374, 2018.
- [13] S. Chapman. On the law of distribution of molecular velocities, and on the theory of viscosity and thermal conduction, in a non-uniform simple monatomic gas. *Phil. Trans. R. Soc. A*, 216(538–548):279–348, 1916.

$\eta = 7$										
0.0008	0.1037	-0.1049	-0.3554	0.0014	0.3359	0.6875	0.2591	-0.0778	-0.4526	-0.2974
-0.2381	-0.3980	0.1920	0.1068	0.1569	0.0292	-0.0194	0.2124	0.2032	-0.1406	-0.0080
-0.1119	-0.1658	0.0497	0.0015	-0.0017	0.0026	-0.0005	0.0762	0.0694	0.0705	-0.0462
0.0447	-0.0373	-0.0667	-0.0105	-0.0732	0.0153	0.0116	-0.0420	-0.0420	-0.0415	0.0246
0.0803	-0.0237	-0.0238	-0.0885	-0.0003	-0.3693	-0.1784	0.2070	0.0048	-0.0340	-0.1100
-0.0015	0.0026	0.0031	-0.0012	0.0009	0.0009	×	×	×	×	×
$\eta = 10$										
0.0023	0.1666	-0.1119	-0.4234	0.0039	0.5006	1.0827	0.3893	-0.1230	-0.7539	-0.4336
-0.3671	-0.6176	0.3035	0.1712	0.2586	0.0483	-0.0322	0.3484	0.3220	-0.2303	-0.0089
-0.1619	-0.2606	0.0956	-0.0254	-0.0049	0.0074	-0.0021	0.1181	0.1099	0.1130	-0.0723
0.0779	-0.0600	-0.1094	-0.0257	-0.1209	0.0275	0.0156	-0.0636	-0.0637	-0.0627	0.0402
0.1322	-0.0361	-0.0362	-0.1341	-0.0008	-0.5668	-0.2818	0.3422	0.0037	-0.0527	-0.1698
-0.0039	0.0075	0.0087	-0.0035	0.0025	0.0025	×	×	×	×	×
$\eta = 17$										
0.0042	0.2193	-0.0840	-0.3948	0.0073	0.6105	1.3974	0.4799	-0.1590	-1.0247	-0.5195
-0.4656	-0.7863	0.3925	0.2244	0.3483	0.0651	-0.0434	0.4683	0.4188	-0.3101	-0.0072
-0.1928	-0.3370	0.1438	-0.0662	-0.0093	0.0140	-0.0045	0.1497	0.1423	0.1483	-0.0927
0.1099	-0.0791	-0.1468	-0.0446	-0.1632	0.0398	0.0169	-0.0787	-0.0790	-0.0776	0.0536
0.1779	-0.0450	-0.0452	-0.1665	-0.0012	-0.7144	-0.3660	0.4618	-0.0001	-0.0667	-0.2146
-0.0067	0.0143	0.0161	-0.0065	0.0048	0.0048	×	×	×	×	×
$\eta = \infty$										
0.0077	0.2861	-0.0063	-0.2555	0.0139	0.7069	1.7691	0.5681	-0.2012	-1.3933	-0.5912
-0.5779	-0.9772	0.4972	0.2897	0.4675	0.0871	-0.0581	0.6297	0.5374	-0.4198	-0.0016
-0.2184	-0.4310	0.2172	-0.1426	-0.0176	0.0264	-0.0087	0.1839	0.1806	0.1921	-0.1165
0.1566	-0.1037	-0.1963	-0.0773	-0.2199	0.0580	0.0154	-0.0933	-0.0940	-0.0920	0.0709
0.2392	-0.0539	-0.0543	-0.1986	-0.0015	-0.8759	-0.4699	0.6216	-0.0097	-0.0820	-0.2630
-0.0111	0.0271	0.0295	-0.0120	0.0092	0.0092	×	×	×	×	×

Table 7: Coefficients $\Lambda_i^{(\eta)}$ in (C.2) for different η .

- [14] S. Chapman and T. G. Cowling. *The Mathematical Theory of Non-uniform Gases, Third Edition*. Cambridge University Press, 1990.
- [15] G. Dimarco, R. Loubère, J. Narski, and T. Rey. An efficient numerical method for solving the Boltzmann equation in multidimensions. *J. Comput. Phys.*, 353:46–81, 2018.
- [16] W. Dreyer. Maximisation of the entropy in non-equilibrium. *J. Phys. A: Math. Gen.*, 20(18):6505–6517, 1987.
- [17] D. Enskog. The numerical calculation of phenomena in fairly dense gases. *Arkiv Mat. Astr. Fys.*, 16(1):1–60, 1921.
- [18] H. Grad. On the kinetic theory of rarefied gases. *Comm. Pure Appl. Math.*, 2(4):331–407, 1949.
- [19] H. Grad. Principles of the kinetic theory of gases. *Handbuch der Physik*, 12:205–294, 1958.
- [20] V. K. Gupta and M. Torrillon. Automated Boltzmann collision integrals for moment equations. *AIP Conference Proceedings*, 1501(1):67–74, 2012.
- [21] S. Harris. *An Introduction to the Theory of the Boltzmann equation*. Dover Publications, 1971.
- [22] Z. Hu and Z. Cai. Burnett spectral method for high-speed rarefied gas flows, 2019. In preparation.

- [23] S. Jin and M. Slemrod. Regularization of the Burnett equations via relaxation. *J. Stat. Phys.*, 103(5–6):1009–1033, 2001.
- [24] K. Kumar. Polynomial expansions in kinetic theory of gases. *Ann. Phys.*, 37(1):113–141, 1966.
- [25] K. Kumar. Polynomial expansions in kinetic theory of gases. *Ann. Phys.*, 37:113–141, 1966.
- [26] C. D. Levermore. Moment closure hierarchies for kinetic theories. *J. Stat. Phys.*, 83(5–6):1021–1065, 1996.
- [27] J. McDonald and M. Torrilhon. Affordable robust moment closures for CFD based on the maximum-entropy hierarchy. *J. Comput. Phys.*, 251:500–523, 2013.
- [28] E. Meyer and G. Sessler. Schallausbreitung in Gasen bei hohen Frequenzen und sehr niedrigen Drucken. *Z. Phys.*, 149(1):15–39, 1957.
- [29] C. Mouhot and R. M. Strain. Spectral gap and coercivity estimates for linearized Boltzmann collision operators without angular cutoff. *J. Math. Pures Appl.*, 87(5):515–535, 2007.
- [30] I. Müller and T. Ruggeri. *Rational Extended Thermodynamics, Second Edition*, volume 37 of *Springer tracts in natural philosophy*. Springer-Verlag, New York, 1998.
- [31] R. S. Myong. Thermodynamically consistent hydrodynamic computational models for high-knudsen-number gas flows. *Phys. Fluids*, 11(9):2788–2802, 1999.
- [32] S. Reinecke and G. M. Kremer. Method of moments of Grad. *Phys. Rev. A*, 42(2):815–820, 1990.
- [33] M. Sh. Shavaliyev. Super-Burnett corrections to the stress tensor and the heat flux in a gas of Maxwellian molecules. *J. Appl. Maths. Mechs.*, 57(3):573–576, 1993.
- [34] H. Struchtrup. Derivation of 13 moment equations for rarefied gas flow to second order accuracy for arbitrary interaction potentials. *Multiscale Model. Simul.*, 3(1):221–243, 2005.
- [35] H. Struchtrup. *Macroscopic Transport Equations for Rarefied Gas Flows: Approximation Methods in Kinetic Theory*. Springer, 2005.
- [36] H. Struchtrup and M. Torrilhon. Regularization of Grad’s 13 moment equations: Derivation and linear analysis. *Phys. Fluids*, 15(9):2668–2680, 2003.
- [37] H. Struchtrup and M. Torrilhon. Regularized 13 moment equations for hard sphere molecules: Linear bulk equations. *Phys. Fluids*, 25:052001, 2013.
- [38] H. Struchtrup and M. Torrilhon. H-theorem, regularization, and boundary conditions for linearized 13 moment equations. *Phys. Rev. Lett.*, 99:014502, 2017.
- [39] P. L. Tallec and J. P. Perlat. Numerical analysis of Levermore’s moment system. Rapport de recherche 3124, INRIA Rocquencourt, March 1997.
- [40] M. Yu. Timokhin, H. Struchtrup, A. A. Kokhanchik, and Ye. A. Bondar. Different variants of R13 moment equations applied to the shock-wave structure. *Phys. Fluids*, 29:037105, 2017.
- [41] I. M. Torrens. *Interatomic Potentials*. Academic Press, 1972.

- [42] M. Torrilhon. Two dimensional bulk microflow simulations based on regularized Grad's 13-moment equations. *SIAM Multiscale. Model. Simul.*, 5(3):695–728, 2006.
- [43] M. Torrilhon. H-theorem for nonlinear regularized 13-moment equations in kinetic gas theory. *Kin. Rel. Models*, 5(1):185–201, 2012.
- [44] M. Torrilhon and H. Struchtrup. Regularized 13-moment equations: shock structure calculations and comparison to Burnett models. *J. Fluid Mech.*, 513:171–198, 2004.
- [45] M. Torrilhon and H. Struchtrup. Boundary conditions for regularized 13-moment-equations for micro-channel-flows. *J. Comput. Phys.*, 227(3):1982–2011, 2008.
- [46] P. Valentini and T. E. Schwartzentruber. Large-scale molecular dynamics simulations of normal shock waves in dilute argon. *Phys. Fluids*, 21(6):066101, 2009.
- [47] W. Vincenti, C. Kruger, and T. Teichmann. Introduction to physical gas dynamics. *Phys. Today*, 19(10):95–95, 1966.